



# Synthesis of highly coke resistant Ni nanoparticles supported MgO/ZnO catalyst for reforming of methane with carbon dioxide



Rajib Kumar Singha<sup>a</sup>, Aditya Yadav<sup>a</sup>, Ayush Agrawal<sup>a</sup>, Astha Shukla<sup>a</sup>, Shubhadeep Adak<sup>a</sup>, Takehiko Sasaki<sup>b</sup>, Rajaram Bal<sup>a,\*</sup>

<sup>a</sup> Nanocatalysis Area, Refining Technology Division, CSIR-Indian Institute of Petroleum, Dehradun 248005, India

<sup>b</sup> Department of Complexity Science and Engineering, Graduate School of Frontier Sciences, The University of Tokyo, Kashiwanoha, Kashiwa-shi, Chiba 277-8561, Japan

## ARTICLE INFO

### Article history:

Received 14 December 2015

Received in revised form 11 March 2016

Accepted 14 March 2016

Available online 15 March 2016

### Keywords:

Ni nanoparticles

Nanocrystalline zinc oxide

Methane

Carbon dioxide reforming

Synthesis gas

## ABSTRACT

Ni-nanoparticles supported on MgO promoted nanocrystalline zinc oxide catalyst was prepared by hydrothermal method in presence of cationic surfactant cetyltrimethylammonium bromide. The catalyst showed very good activity for the reforming of methane with carbon dioxide to produce synthesis gas, where H<sub>2</sub>/CO ratio was almost 1 and the catalyst showed no deactivation for more than 100 h. The prepared catalyst was characterized using the analytical techniques like N<sub>2</sub>-physisorption studies, X-ray diffraction (XRD), Scanning electron microscopy (SEM), Transmission electron microscopy (TEM), Temperature programmed desorption (TPD), Temperature programmed reduction (TPR), Temperature programmed oxidation (TPO), H<sub>2</sub>-chemisorption, Thermo-gravimetric analysis (TGA), Inductively coupled plasma atomic emission spectroscopy (ICP-AES), X-ray photoelectron spectroscopy (XPS), and Extended X-ray absorption fine structure (EXAFS). Transmission electron microscopy and H<sub>2</sub>-chemisorption analysis indicated that highly dispersed Ni nanoparticles with average size 5.7 nm, present on ZnO when MgO was added with the catalyst. The strong Ni–ZnO interaction was evidenced from TPR and EXAFS analysis. The presence of highly dispersed Ni nanoparticles and strong metal support interaction enhanced the reduction behaviour of the Ni–MgO/ZnO catalyst. The presence of MgO increased the adsorption behaviour of CO<sub>2</sub>, enhanced the dissociation of CO<sub>2</sub> and accelerated the carbon elimination.

© 2016 Elsevier B.V. All rights reserved.

## 1. Introduction

Protection of the environment is a topic of fundamental importance of mankind. Developed countries and the developing ones have come together to establish national programs to fight against the various source of pollution [1]. The unquestionable importance of catalytic transformation of methane and carbon dioxide from both industrial and environmental point of view attracted the researchers to convert them into synthesis gas or other valuable chemicals. The main and attractive feature of the dry reforming reaction is both the reaction feed, CH<sub>4</sub> as well as CO<sub>2</sub> are greenhouse gasses with methane having about 20 times much more greenhouse potential than CO<sub>2</sub>. So, from the environmental point of view, this is a very important process where both the greenhouse gasses can be converted to synthesis gas, which can be used for the production of chemicals like methanol and fuels via Fischer–Tropsch (FT) syn-

thesis [2–6]. Steam and dry reforming reactions both have similar thermodynamic characteristics but the coke formation problem is much more in dry reforming than in steam reforming because of the low H<sub>2</sub>/CO ratio [7].

It is a major challenge to develop a suitable catalyst with superior activity for dry reforming of methane. Variety of supports has been investigated using different noble metals like Pt, Pd, Rh, Ru, Ir [8–18] and 1st row transition metals like, Ni, Fe, Co, Cu [19–24] as dry reforming catalysts but due to coke deposition the 1st row transition metal catalysts deactivates very rapidly. Researchers reported high efficiency of noble metal catalysts for dry reforming of methane but the high cost and low abundance restricted the catalyst for commercial implementation [11,25–27]. Though noble metal have found to be less coke sensitive [28–30] but Ni based catalyst are more preferred and need to establish because of its high abundance and low cost. The deposition of coke on the catalyst surface is due to the decomposition of CH<sub>4</sub> and disproportionation of CO during the reaction which causes the reactor plugging [30–32]. So, modification of the Ni catalysts by changing the support or doping which can reduce coke deposition, can be

\* Corresponding author.

E-mail addresses: [rajab.73@yahoo.com](mailto:rajab.73@yahoo.com), [raja@iip.res.in](mailto:raja@iip.res.in) (R. Bal).

a viable alternative for the commercial application of the Ni-based catalysts for the methane reforming with CO<sub>2</sub> [33,34]. The catalysts with high Ni dispersion and strong metal support interaction are found to be coke resistive and catalytically superior for the methane dry reforming reaction [21,35,36]. Basic promoters like MgO, La<sub>2</sub>O<sub>3</sub> was also reported to resist coke deposition due to their basic character which favors the carbon removal mechanism during catalytic reaction [21,36,38–40]. Sodesawa et al. [41] investigated different stoichiometric feed ratio over several catalysts and found that most of the catalysts get deactivated due to the coke deposition.

Synthesis gas is suitable for the direct production of DME and Fischer–Tropsch process. Earlier reports suggested that Nickel is an active metal for the catalytic reforming process but coke deposition deactivates the catalysts very fast [42–46]. Nowadays, it has been found that catalyst in the nanosize domain (especially for the supported nanoparticles) shows superior catalytic activity due to high dispersion, presence of metal support interaction, synergistic effect and high surface area. Recently, we have developed new synthetic strategies to synthesize nanomaterials with very small sizes [47–52]. The present report describes the catalytic activity of Ni-nanoparticles supported on MgO promoted ZnO nanocrystals prepared by hydrothermal method for reforming of methane with CO<sub>2</sub>. The catalyst showed very good catalytic activity for CO<sub>2</sub> reforming of methane to produce synthesis gas with H/C mole ratio almost 1, without any deactivation till 100 h.

## 2. Experimental

### 2.1. Catalyst preparation

#### 2.1.1. Preparation of Ni–ZnO

Ni–ZnO catalyst was prepared by hydrothermal method. In a typical synthesis of Ni–ZnO catalyst, mole ratio of the homogeneous precursor salt solution of Ni(NO<sub>3</sub>)<sub>2</sub>·6H<sub>2</sub>O:Zn(NO<sub>3</sub>)<sub>2</sub>·6H<sub>2</sub>O:H<sub>2</sub>O was kept at 1:14:650 and stirred for 1 h. Then 20 ml of 0.25 (M) ethanolic CTAB solution was mixed with 60 ml of homogeneous aqueous precursor salt solution and continued stirring for one more hour. After, 1 h of stirring 2 ml of NH<sub>2</sub>NH<sub>2</sub>·H<sub>2</sub>O was added keeping the mole ratio of Ni:NH<sub>2</sub>NH<sub>2</sub> to 1. 1(M) Na<sub>2</sub>CO<sub>3</sub> solution was used to maintain the pH of the whole mixture solution at 10. The mixture was continued stirring for one more hour to form a gel like mixture. The whole mixture was then put into an autoclave and kept at 180 °C for 24 h. The autoclave was then cooled to room temperature and the precipitate was washed with water and dried at 100 °C for 12 h. The obtained solid was calcined at 550 °C in air. The catalyst was designated as wt%Ni–ZnO<sup>HT</sup>.

#### 2.1.2. Preparation of Ni–MgO–ZnO

In a typical preparation method MgO promoted Ni-nanoparticles supported on ZnO was prepared by the following method. A homogeneous precursor salt solution was prepared by using a definite mole ratio of the precursor salts. Here in this preparation method the mole ratio of Ni(NO<sub>3</sub>)<sub>2</sub>·6H<sub>2</sub>O:Zn(NO<sub>3</sub>)<sub>2</sub>·6H<sub>2</sub>O:Mg(NO<sub>3</sub>)<sub>2</sub>·6H<sub>2</sub>O:H<sub>2</sub>O was kept at (0.5–1.5):14:0.7:650. After 1 h of stirring, 20 ml of 0.25 (M) ethanolic CTAB solution was mixed with 60 ml of homogeneous aqueous precursor salt solution and continued stirring for one more hour. After, 1 h of stirring 2 ml of NH<sub>2</sub>NH<sub>2</sub>·H<sub>2</sub>O was added keeping the mole ratio of Ni:NH<sub>2</sub>NH<sub>2</sub> to 1. Then the pH of the whole mixture solution was maintained at 10 using 1(M) Na<sub>2</sub>CO<sub>3</sub> solution. The mixture was continued stirring for one more hour to form a gel like mixture. The whole mixture was then put into an autoclave and kept at 180 °C for 24 h. The autoclave was then cooled to room temperature and the precipitate was washed with water and dried

at 100 °C for 12 h. The obtained solid was calcined at 550 °C in air. The catalyst was denoted as wt%Ni–wt%MgO/ZnO<sup>HT</sup>.

For comparison purpose Ni was impregnated on commercial ZnO, hydrothermally prepared ZnO and the catalysts were denoted as wt%Ni–ZnO<sup>ImpCom</sup>, wt%Ni–ZnO<sup>Imp</sup> (Supporting information).

### 2.2. Catalyst Characterization

The surface area analysis of the prepared samples were done at –196 °C with a Belsorbmax (BEL, Japan) using the BET equation. Degasification of the sample was done at 350 °C for 6 h before analysis. Powder X-ray diffraction patterns of the samples were recorded on a Rigaku–Geigerflex X-ray diffractometer fitted with a Cu K $\alpha$  radiation source. The X-ray diffraction patterns of all the samples were recorded in 10°–80° region with a 0.04 step size (step time=4 s). Incorporation of Ni into the catalyst were examined by comparing the XRD patterns of prepared ZnO, 2.3Ni–4.3MgO/ZnO<sup>HT</sup>, 4.8Ni–4.3MgO/ZnO<sup>HT</sup> and other samples. Thermal stability of the catalysts, was checked from the XRD pattern of the after reaction catalyst compared with the XRD pattern of fresh catalyst. To check the reducibility of the catalysts, TPR experiments for the samples were carried out in a Micromeritics, Auto Chem II 2920 instrument connected with a thermal conductivity detector (TCD). TPR analysis for all the samples were done in the temperature range of 40–1000 °C with an increment of 10 °C min<sup>–1</sup>, using helium as carrier gas. SEM images of the prepared samples were taken on a FEI Quanta 200 F, using a tungsten filament doped with lanthanum hexaboride (LaB<sub>6</sub>) as the X-ray source, fitted with an ETD detector with high vacuum mode, using secondary electrons and an acceleration tension of 10 or 30 kV. Analysis of the samples was done by spreading them on a carbon tape. Elemental analysis of the samples was carried out by energy dispersive X-ray spectroscopy (EDX). Distribution of all the elements of the catalyst was also checked by elemental mapping, using the same spectrophotometer. TEM images of the prepared samples were collected using a Jeol JEM 2100 microscope. The samples were prepared by mounting an ethanol-dispersed sample on a lacey carbon Formvar coated Cu grid. Thermo Scientific K-Alpha X-ray photoelectron spectrometer was used for X-ray photoelectron spectra (XPS) of the samples and binding energies ( $\pm 0.1$  eV) were determined with the reference peak position of C 1s at 284.8 eV. The XPS spectra of the O 1s, C 1s, Ni 2p, Zn 2p regions were measured. Calibration of the binding energy (BE) scale was done by using the C 1s (BE = 284.6 eV) signal. EXAFS measurements of the Ni K-edge were carried out at the High Energy Accelerator Research Organization (KEK-IMMS-PF). XAFS analysis was done in transition mode and spectra were taken at BL-7C and BL-9C. The electron storage ring was operated at 2.5 GeV and 450 mA and synchrotron radiation from the storage ring was monochromatized by a Si (111) channel cut crystal. The ionized chambers, used as detectors for the incident X-ray (I<sub>0</sub>) and transmitted X-ray (I), were filled with N<sub>2</sub> gas mixture, respectively. Cu foil was used to calibrate the angle of the monochromators. UWXAFS analysis package [53] including background subtraction program AUTOBK [54] and curve fitting program FEFFIT [55] was used to analyze the EXAFS raw data. The amplitude reducing factor, S<sub>0</sub><sup>2</sup> was fixed at 1.0. FEFF 8.4 code [56] was used for the theoretical calculation of the backscattering amplitude and phase shift.

### 2.3. Catalyst activity measurement

The dry reforming of methane was carried out in a fixed-bed down flow reactor at atmospheric pressure. Before reaction, all the catalysts were reduced at 600 °C for 2 h in presence of 20% H<sub>2</sub> balanced He gas. Typically, 120 mg of catalyst was placed in between two quartz wool plugged in the centre of the 6 mm quartz tube reactor. Dry reforming of methane was carried out at different tem-

**Table 1**  
Physico-chemical properties of the catalysts.

Sr. No.	Catalyst	Surface Area (m <sup>2</sup> /g)	Ni Dispersion (%)
1	Commercial ZnO	3.2	
2	ZnO <sup>HT</sup>	33.5	
3	4.3MgO/ZnO <sup>HT</sup>	44.3	
4	5Ni-ZnO <sup>ImpCom</sup>	5.9	3.1
5	5Ni-ZnO <sup>Imp</sup>	7.7	3.6
6	4.7Ni-ZnO <sup>HT</sup>	38.6	7.3
7	2.3Ni-4.3MgO/ZnO <sup>HT</sup>	48.6	21.4
8	4.8Ni-4.3MgO/ZnO <sup>HT</sup>	53.2	19.6
9	9.2Ni-4.5MgO/ZnO <sup>HT</sup>	53.7	10.2

perature (450–800 °C). The gas hourly space velocity (GHSV) was varied between 10000 mlg<sup>-1</sup> h<sup>-1</sup> to 50000 mlg<sup>-1</sup> h<sup>-1</sup> with a molar ratio of CH<sub>4</sub>:CO<sub>2</sub>:He of 1:1:12. The reaction products were analyzed using an online gas chromatography (Agilent 7890A) fitted with a TCD detector using two different columns Molecular sieves (for analysing H<sub>2</sub>) and PoraPack-Q (for analysing CH<sub>4</sub>, CO<sub>2</sub> and CO). Kinetic experiments were carried out at 480–520 °C, where methane and CO<sub>2</sub> conversion was less than 15% with different feed ratios. Conversion of CH<sub>4</sub> and CO<sub>2</sub> was measured using the following equations:

$$X_{CH_4} (\%) = \frac{F_{CH_4;in} - F_{CH_4;out}}{F_{CH_4;in}} \times 100$$

$$X_{CO_2} (\%) = \frac{F_{CO_2;in} - F_{CO_2;out}}{F_{CO_2;in}} \times 100$$

where  $X_{CH_4} (\%)$  and  $X_{CO_2} (\%)$  are the conversion of methane and CO<sub>2</sub>.  $F_{CH_4;in}$ ,  $F_{CH_4;out}$  are the inlet and outlet flows of methane.  $F_{CO_2;in}$ ,  $F_{CO_2;out}$  are the inlet and outlet flows of CO<sub>2</sub>.

### 3. Results

#### 3.1. Characterization

##### 3.1.1. Physicochemical properties of the Catalyst

The estimation of Ni was carried out by ICP-AES. In Table 1, surface area, Ni-dispersion and wt% of Ni of different samples are shown. The surface area of the prepared ZnO, 4.7Ni-ZnO<sup>HT</sup>, 2.3Ni-4.3MgO/ZnO<sup>HT</sup>, 4.8Ni-4.3MgO/ZnO<sup>HT</sup> and 9.2Ni-4.5MgO/ZnO<sup>HT</sup> catalyst (4.8Ni-4.3MgO/ZnO<sup>HT</sup>) was done and compared. The BET surface area of prepared ZnO was also compared with the commercial ZnO. The surface area of commercial ZnO was 3.2 m<sup>2</sup>/g whereas the BET surface area of prepared Zinc oxide was found to be 33.5 m<sup>2</sup>/g. Addition of MgO further increased the BET surface area of the sample. 4.3MgO-ZnO<sup>HT</sup> sample showed surface area 44.3 m<sup>2</sup>/g. The reason for the increase in surface area with addition of MgO may be due to the low density of MgO and formation of smaller catalyst particles. With the addition of MgO, the decrease in catalyst particle size increased the surface to volume ratio and the catalyst showed higher surface area. BET surface area of the catalysts was increased with increasing wt% of Ni loading. 2.3Ni-4.3MgO/ZnO<sup>HT</sup>, 4.8Ni-4.3MgO/ZnO<sup>HT</sup>, 9.2Ni-4.5MgO/ZnO<sup>HT</sup> samples showed surface area 48.6 m<sup>2</sup>/g, 53.2 m<sup>2</sup>/g and 53.7 m<sup>2</sup>/g respectively. The increasing surface area also indicated that the size of the catalyst decreasing with addition of MgO and Ni. Earlier reports also supported the observation of increasing surface area with increasing metal loading [57]. Number of Ni particles on the surface of the 4.8Ni-4.3MgO/ZnO<sup>HT</sup> catalyst was calculated to be  $1.28 \times 10^{17}$  per g catalyst having average Ni particle size 5.67 nm.

##### 3.1.2. X-ray diffraction (XRD)

XRD pattern of the prepared NiO, 4.6Ni-MgO<sup>HT</sup>, 5Ni-ZnO<sup>ImpCom</sup>, 5Ni-ZnO<sup>Imp</sup>, 4.7Ni-ZnO<sup>HT</sup>, 2.3Ni-4.3MgO-ZnO<sup>HT</sup>,

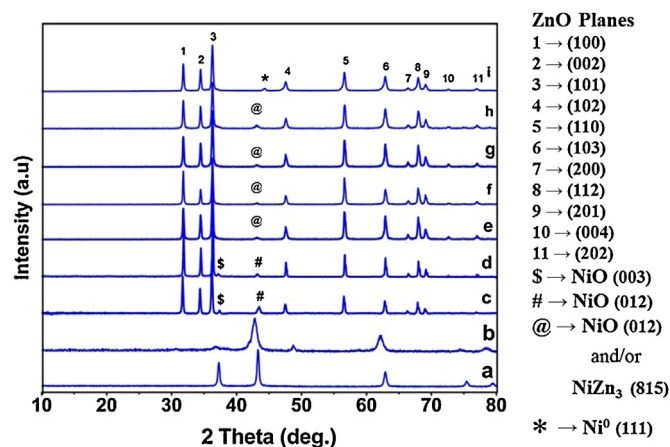


**Fig. 1.** XRD pattern of (a) NiO, (b) 4.6Ni-MgO<sup>HT</sup>, (c) 5Ni-ZnO<sup>ImpCom</sup>, (d) 5Ni-ZnO<sup>Imp</sup>, (e) 4.7Ni-ZnO<sup>HT</sup>, (f) 2.3Ni-4.3MgO/ZnO<sup>HT</sup>, (g) 4.8Ni-4.3MgO/ZnO<sup>HT</sup>, (h) 9.2Ni-4.5MgO/ZnO<sup>HT</sup> and (i) spent 4.8Ni-4.3MgO/ZnO<sup>HT</sup> catalysts (after 100 h TOS at 800 °C).

4.8Ni-4.3MgO/ZnO<sup>HT</sup>, 9.2Ni-4.5MgO/ZnO<sup>HT</sup> and spent 4.8Ni-4.3MgO/ZnO<sup>HT</sup> (TOS=100 h, Temp. 800 °C) catalysts are shown in Fig. 1a–i respectively. The XRD peaks of 5Ni-ZnO<sup>ImpCom</sup> (Fig. 1c), 5Ni-ZnO<sup>Imp</sup> (Fig. 1d), 4.7Ni-ZnO<sup>HT</sup> (Fig. 1e), 2.3Ni-4.3MgO/ZnO<sup>HT</sup> (Fig. 1f), 4.8Ni-4.3MgO/ZnO<sup>HT</sup> (Fig. 1g) and 9.2Ni-4.5MgO/ZnO<sup>HT</sup> (1 h) are attributed to Zinc Oxide (JCPDS Card No. 36-1451) and NiO (JCPDS Card No. 47-1049). The XRD peak at 43.3° was due to the NiO particles formed during synthesis of the catalysts. The XRD peak observed from XRD was at  $2\theta = 43.3^\circ$  which is exactly the match with JCPDS Card No. 47-1049 for NiO whereas the formation of NiO–MgO solid solution shifts NiO XRD peak to a lower Bragg angles [24,58]. So there was no NiO–MgO solid solution formation. The low temperature (550 °C) calcination of the catalyst could be a reason for the absence of Ni–MgO solid solution in the fresh Ni-MgO/ZnO<sup>HT</sup> catalysts. Jiang et al. [59] have claimed that addition of Ti reduced the possibility of Ni–MgO solid solution formation in Ni/Mg<sub>x</sub>Ti<sub>1-x</sub>O catalyst, where the calcination temperature of the catalyst was 650 °C. So, it could also be a possibility that the presence of ZnO hindered the Ni–MgO solid solution formation for fresh Ni-MgO/ZnO<sup>HT</sup> catalysts. The Ni impregnated Commercial ZnO catalyst (5Ni-ZnO<sup>ImpCom</sup>) showed NiO peaks at  $2\theta$  value 37.2° and 43.3°. The XRD peaks of the catalysts containing MgO (Fig. 1f–i) did not show any characteristic peak for MgO. The reason may be due to the low loading of MgO. From the XRD pattern of 2.3Ni-4.3MgO/ZnO<sup>HT</sup>, 4.8Ni-4.3MgO/ZnO<sup>HT</sup>, 9.2Ni-4.5MgO/ZnO<sup>HT</sup> (Fig. 1f–h), it was observed that, as the Ni loading increases the peak intensity at  $2\theta$  value 43.4° increases. The peak at  $2\theta$  value 43.4° can also be due to the NiZn<sub>3</sub> species (JCPDS Card No. 47-1019). The catalysts showed characteristic peaks of ZnO (JCPDS Card No. 36-1451) at  $2\theta$  value 31.77°, 34.42°, 36.25°, 47.54°, 56.60°, 62.86°, 66.4°, 67.96°, 69.10° due to its (100), (002), (101), (102), (110), (103), (200), (112) and (201) planes. The crystallite size of ZnO was obtained using Scherrer equation and the average particle size was found to be 112 nm. During catalyst preparation it is a possibility that part of Ni or MgO could dissolve into ZnO framework. But from XRD we calculated the lattice parameter of ZnO for Ni–MgO–ZnO catalysts. We found that the lattice parameters ( $a=b=3.25$ ,  $c=5.20$ ) was exactly same as obtained from JCPDS Card 36-1451 for ZnO. Insertion of Ni or MgO in the framework of ZnO could have changed the lattice parameters for ZnO. So, unchanged lattice parameters indicated that there was no insertion of Ni or MgO into the ZnO framework. The XRD of the spent catalyst reveals that the phases of ZnO nanoparticles were unchanged which showed the thermal

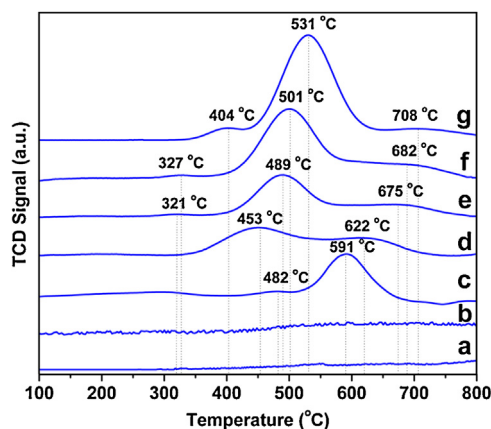


**Fig. 2.**  $H_2$ -TPR profile of (a)  $ZnO^{HT}$ , (b)  $MgO^{HT}$ , (c) 4.8Ni- $MgO^{HT}$ , (d) 4.7Ni- $ZnO^{HT}$ , (e) 2.3Ni-4.3MgO/ $ZnO^{HT}$ , (f) 4.8Ni-4.3MgO/ $ZnO^{HT}$  and (g) 9.2Ni-4.5MgO/ $ZnO^{HT}$  catalyst.

stability of the catalyst. The XRD of the spent 4.8Ni-4.3MgO/ $ZnO^{HT}$  (Fig. 1i) catalyst (TOS—100 h, Temp. 800 °C) showed the presence of metallic Ni in the catalyst. The reason for the presence of metallic Ni was the insitu reduction by the produced  $H_2$  during the catalytic process. Even after TOS reaction at 800 °C, the absence of Ni-MgO solid solution in 4.8Ni-4.3MgO/ $ZnO^{HT}$  catalyst also indicated the possibility of the reason that ZnO may have hindered the Ni-MgO solid solution formation.

### 3.1.3. $H_2$ -temperature programmed reduction ( $H_2$ -TPR) and $H_2$ -chemisorption

The reducibility of the catalysts were examined by  $H_2$ -TPR. Table 2 shows the consumption of hydrogen during TPR analysis. The  $H_2$ -TPR of 4.7Ni- $ZnO^{HT}$ , 2.3Ni-4.3MgO/ $ZnO^{HT}$  and 4.8Ni-4.3MgO/ $ZnO^{HT}$  and 9.2Ni-4.5MgO/ $ZnO^{HT}$  catalyst are shown in Fig. 2.  $MgO$  and  $ZnO$  reduces at very high temperatures ( $>800^\circ C$ ) (Fig. 2a,b) which is higher than our reaction temperature [60,61]. 4.8Ni- $MgO$  showed the reduction peak at 482 °C and 591 °C due to the highly interacted Ni species with  $MgO$  (Fig. 2c). The reduction peak of Ni species did not give any indication of NiO- $MgO$  solid solution. Formation of NiO- $MgO$  solid solution would have shifted the reduction temperature of NiO to a much higher temperature (above 750 °C) [24,32,36,62].  $H_2$ -TPR of 4.7Ni- $ZnO^{HT}$  catalyst (Fig. 2d) showed two distinct peaks at 453 °C and at 622 °C which was due to the consumption of  $H_2$  by NiO species. The first peak at 453 °C was due to the reduction of surface NiO to metallic Ni and the second peak at 622 °C was due to the reduction of bulk NiO to metallic Ni [63]. The reduction peaks clearly indicated the formation of two type of NiO species reducible at different temperatures. Addition of  $MgO$  changed the reducibility of the catalysts. 2.3Ni-4.3MgO/ $ZnO^{HT}$  (Fig. 2e), 4.8Ni-4.5MgO/ $ZnO^{HT}$  (Fig. 2f) and 9.2Ni-4.5MgO/ $ZnO^{HT}$  (Fig. 2g) catalyst showed three reduction peaks. 2.3Ni-4.3MgO/ $ZnO^{HT}$  catalyst showed reduction peaks at 321 °C, 489 °C and 675 °C. The reduction peak at 321 °C was due to the free surface NiO species and the other two peaks at 489 °C, 675 °C are due to the reduction of NiO species present in the surface interacting with the  $ZnO$  support. The 4.8Ni-4.3MgO/ $ZnO^{HT}$  catalyst showed same reducibility behavior and the reduction peaks were shifted towards a bit higher temperature. The 4.8Ni-4.3MgO/ $ZnO^{HT}$  catalyst showed three reduction peaks at 327 °C, 501 °C and 682 °C. We have also carried out metal dispersion analysis for the prepared catalysts by  $H_2$ -chemisorption method. 4.7Ni- $ZnO^{HT}$  catalyst showed Ni dispersion of 7.3% but with the addition of  $MgO$ , the dispersion was increased almost 3 times to 19.6%. Earlier reports also suggested that presence of a basic component ( $MgO$ ) in the catalyst system increases the metal dispersion of the catalyst [37,38,64,65].

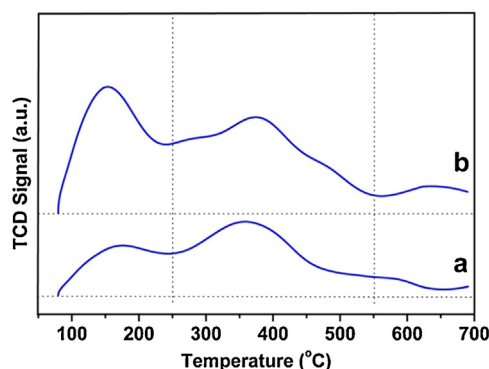


**Fig. 3.**  $CO_2$ -TPD profile of (a) 4.7Ni- $ZnO^{HT}$  and (b) 4.8Ni-4.3MgO/ $ZnO^{HT}$  catalysts.

### 3.1.4. $CO_2$ -temperature programmed desorption ( $CO_2$ -TPD)

$CO_2$ -TPD plots of 4.7Ni- $ZnO^{HT}$  and 4.8Ni-4.3MgO/ $ZnO^{HT}$  catalysts are shown in Fig. 3. From the  $CO_2$  TPD plots of 4.7Ni- $ZnO^{HT}$  (Fig. 3a) and 4.8Ni-4.3MgO/ $ZnO^{HT}$  (Fig. 3b) catalysts showed that both the catalysts have three types of basic sites. 100–250 °C is the weak basic sites, 250–470 °C is the medium basic sites and above 470 °C is for the strong basic sites. The desorbed amounts of  $CO_2$  molecules are shown in Table 3. The amount of desorbed  $CO_2$  molecules showed that the addition of  $MgO$  increased the basic nature of the catalyst. Most prominent effect of  $MgO$  addition to Ni- $ZnO$  was observed on the surface basicity of the catalyst (100–250 °C). It indicated that the 4.8Ni-4.3MgO/ $ZnO^{HT}$  catalyst provides much more basic sites for the adsorption of acidic  $CO_2$  on the surface of the catalyst compared to the 4.7Ni- $ZnO^{HT}$  catalyst. Earlier reports also revealed that basic catalysts improves the adsorption of acidic  $CO_2$  molecules and supplies surface oxygen to prevent coke deposition [66–69].

### 3.1.5. Scanning Electron microscopy (SEM) and transmission electron microscopy (TEM)

The morphologies of the prepared catalysts were analyzed by scanning electron microscopy (SEM). The SEM images of 5Ni- $ZnO^{ImpCom}$ , 4.7Ni- $ZnO^{HT}$ , 4.8Ni-4.3MgO/ $ZnO^{HT}$  catalyst represented by Fig. 4a–c. The representative SEM images showed the morphological differences of the prepared catalysts. The 5 wt% Ni-Com.  $ZnO^{Imp}$  catalyst showed the non-uniform catalyst particle sizes, 4.7Ni- $ZnO^{HT}$  catalyst showed rod like morphology and 4.8Ni-4.3MgO/ $ZnO^{HT}$  showed nanoparticles in the range of 90–130 nm. So, the morphologies of the prepared catalysts are completely different from the 5Ni- $ZnO^{ImpCom}$  catalyst. The presence of elements Ni, Mg, Zn and O was confirmed by energy dispersive X-ray analysis (EDAX). The EDAX pattern and the elemental composition of 4.8Ni-4.3MgO/ $ZnO^{HT}$  catalyst, obtained from SEM analysis are shown in Fig. 4d,e respectively. The analysis of distribution of elements in the catalyst was carried out by elemental mapping. The elemental mapping of Ni of 4.8Ni-4.3MgO/ $ZnO^{HT}$  catalyst was shown in Fig. 4f which showed almost uniform distribution of Ni particles in the catalyst. Therefore, the change in morphology of the catalyst with addition of  $MgO$  indicated that  $MgO$  plays a crucial role in the morphology development of the catalyst. SEM image of 5Ni- $ZnO^{Imp}$  showed agglomeration of catalyst particles (Supporting information Fig. S1).

Transmission electron microscopic (TEM) images of 4.7Ni- $ZnO^{HT}$ , 4.8Ni-4.3MgO/ $ZnO^{HT}$  and spent 4.8Ni-4.3MgO/ $ZnO^{HT}$  (TOS—100 h, Temp. 800 °C) catalysts are shown in Fig. 5. The TEM image of 4.7Ni- $ZnO^{HT}$  catalyst was shown in Fig. 5a and it showed capsule like morphology of the catalyst. The TEM images of 4.8Ni-4.3MgO/ $ZnO^{HT}$  catalysts represented by Fig. 5b,c showed 5–15 nm Ni particles. The TEM images did not show much difference in mor-

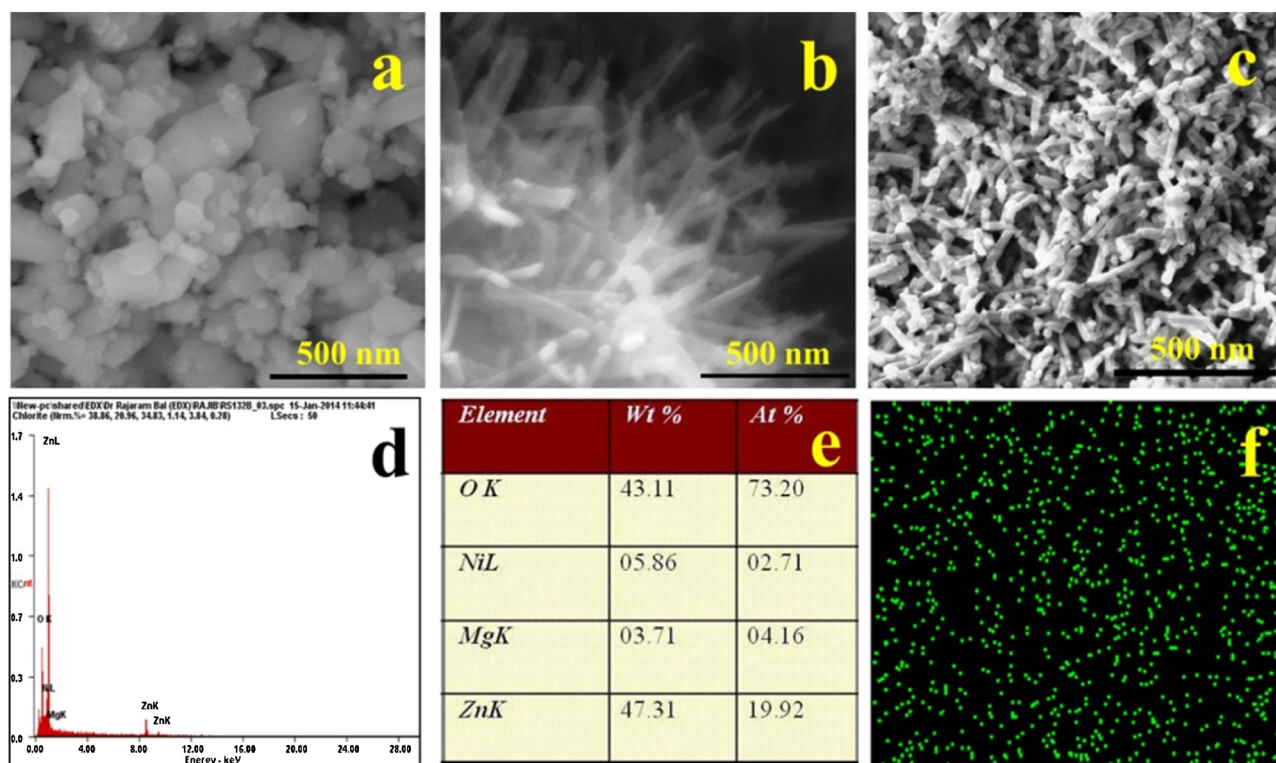


**Fig. 4.** (a) SEM image of 5Ni-ZnOmpCom., (b) SEM image of 4.7Ni-ZnO<sup>HT</sup>, (c) SEM image of 4.8Ni-4.3MgO/ZnO<sup>HT</sup>, (d) EDAX pattern of 4.8Ni-4.3MgO/ZnO<sup>HT</sup> catalyst, (e) Elemental composition of 4.8Ni-4.3MgO/ZnO<sup>HT</sup> catalyst and (f) Mapping of Ni of 4.8Ni-4.3MgO/ZnO<sup>HT</sup> catalyst.

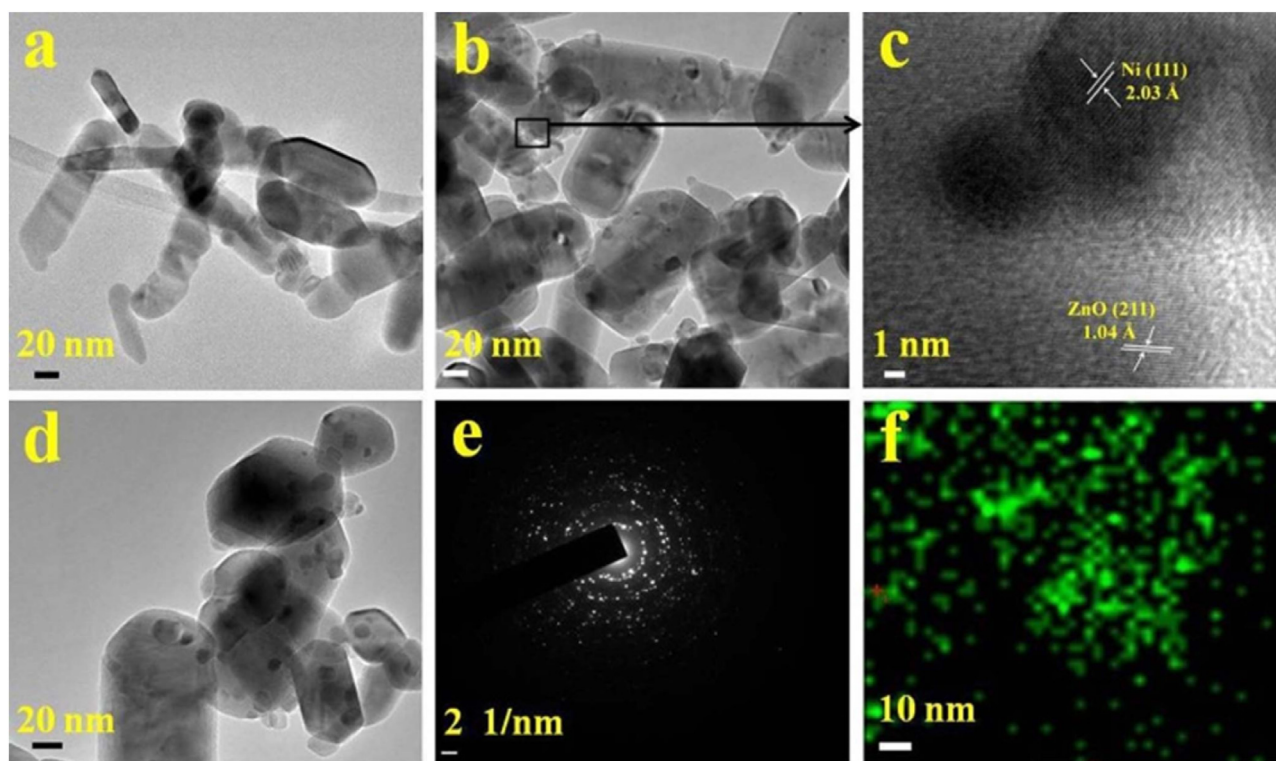


**Fig. 5.** (a) TEM image of 4.7Ni-ZnO<sup>HT</sup>, (b) TEM image of 4.8Ni-4.3MgO/ZnO<sup>HT</sup>, (c) Fringes of ZnO and Ni of .8 wt% Ni- 4.3MgO/ZnO<sup>HT</sup>, (d) TEM image of used 4.8Ni-4.3MgO/ZnO<sup>HT</sup> (after 100 h TOS at 800 °C), (e) SAED pattern of 4.8Ni-4.3MgO/ZnO<sup>HT</sup> catalyst, and (f) Mapping of Ni of 4.8Ni-4.3MgO/ZnO<sup>HT</sup> catalyst.

**Table 2**  
H<sub>2</sub>-consumption during H<sub>2</sub>-TPR of the catalysts.

Sr. No.	Catalyst	Reduction peaks	H <sub>2</sub> uptake (mmol/g)	Total hydrogen consumption (mmol/g)
1	4.7Ni-ZnO <sup>HT</sup>	330–550 °C	0.569727	0.985874
		550–750 °C	0.416147	
2	2.3Ni-4.3MgO/ZnO <sup>HT</sup>	280–350 °C	0.008473	0.607115
		370–590 °C	0.458959	
		590–750 °C	0.139683	
3	4.8Ni-4.3MgO/ZnO <sup>HT</sup>	290–360 °C	0.009726	1.150268
		390–600 °C	1.036710	
		600–750 °C	0.103832	

**Table 3**  
CO<sub>2</sub>-TPD of catalysts.

Entry	Catalyst	wt% of MgO	Desorption peaks	Desorbed CO <sub>2</sub> (mmol/g)	Total desorbed CO <sub>2</sub> (mmol/g)
1	4.7Ni-ZnO <sup>HT</sup>	0	100–250 °C	0.02265	0.09264
			250–550 °C	0.05572	
			above 550 °C	0.01427	
2	4.8Ni-4.3MgO/ZnO <sup>HT</sup>	4.3	100–250 °C	0.04953	0.13046
			250–550 °C	0.06420	
			above 550 °C	0.01673	

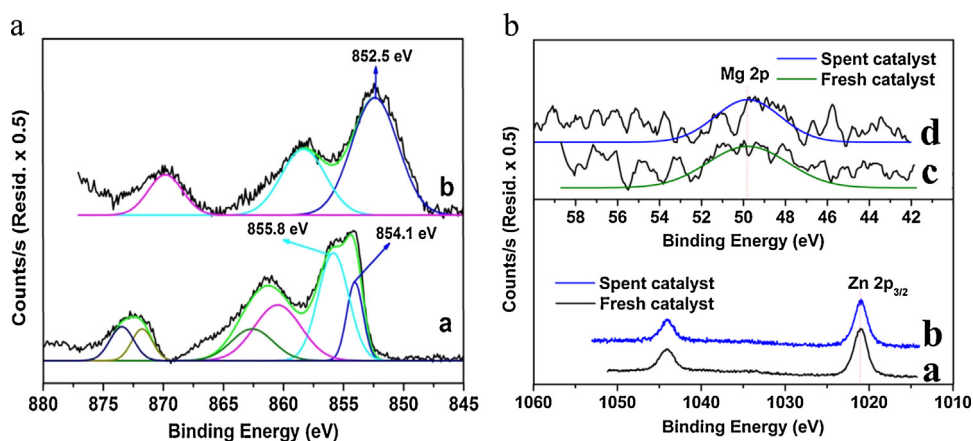


**Fig. 6.** (A) XPS patterns of Ni2p of (a) fresh 4.8Ni-4.3MgO/ZnO<sup>HT</sup> catalyst and (b) spent 4.8Ni-4.3MgO/ZnO<sup>HT</sup> catalyst (after 100 h TOS at 800 °C). (B) XPS patterns of Zn2p (a, b) and Mg2p (c, d) of fresh 4.8Ni-4.3MgO/ZnO<sup>HT</sup> catalyst and spent 4.8Ni-4.3MgO/ZnO<sup>HT</sup> catalyst (after 100 h TOS at 800 °C).

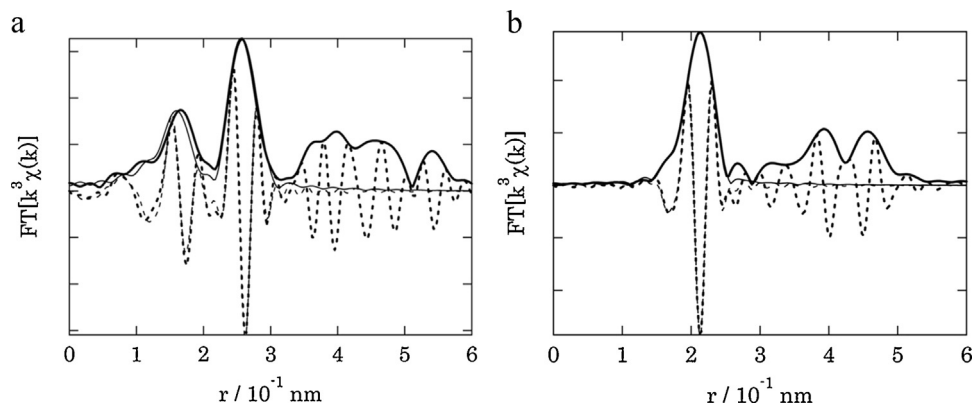


**Fig. 7.** (a) k<sup>3</sup>-weighted Fourier transform of Ni-L<sub>III</sub> edge EXAFS for the fresh 4.8Ni-4.3MgO/ZnO<sup>HT</sup> catalyst. Amplitude and imaginary part are traced by thick curve and thin curve, respectively. Observed data are shown with solid lines and fitting data are shown with dotted lines. (b) k<sup>3</sup>-weighted Fourier transform of Ni-L<sub>III</sub> edge EXAFS for the spent 4.8Ni-4.3MgO/ZnO<sup>HT</sup> catalyst (after 100 h TOS at 800 °C). Amplitude and imaginary part are traced by thick curve and thin curve, respectively. Observed data are shown with solid lines and fitting data are shown with dotted lines.

phology of the 4.7Ni-ZnO<sup>HT</sup>, 4.8Ni-4.3MgO/ZnO<sup>HT</sup> catalysts. The TEM image of the spent catalyst was represented by Fig. 5d which showed the unchanged morphology of the catalyst indicating its thermal stability. The SAED pattern of 4.8Ni-MgO/ZnO<sup>HT</sup> catalyst showed the polycrystalline nature of the sample. Elemental mapping carried out by TEM instrument for the analysis of distribution of Ni of 4.8Ni-4.3MgO/ZnO<sup>HT</sup> catalyst was also shown in Fig. 5f which also showed the homogeneous distribution of Ni particles.

### 3.1.6. X-ray photoelectron spectroscopy (XPS)

The surface of 4.8Ni-4.3MgO/ZnO<sup>HT</sup> catalyst was analysed by X-ray photoelectron spectroscopy. The typical Ni2p core-level spectra of fresh 4.8Ni-4.3MgO/ZnO<sup>HT</sup> and spent 4.8Ni-4.3MgO/ZnO<sup>HT</sup> (TOS—100 h, Temp. 800 °C) catalysts are shown in Fig. 6A. The main purpose of this XPS analysis was to find out the Ni species present on the surface of the catalyst. The peak at binding energy value 854.1 eV and 855.8 eV for Ni2p<sub>3/2</sub> indicates the presence of NiO and Ni<sub>2</sub>O<sub>3</sub> species in the fresh catalyst. The XPS spectra of the spent catalyst showed the peak at 852.5 eV for Ni2p<sub>3/2</sub> confirmed the presence of metallic Ni, which was also supported by the XRD result. The presence of metallic Ni species can be explained by the in situ reduction of the Ni-oxide species to metallic Ni by the H<sub>2</sub> produced during the reforming reaction. The XPS pattern of Mg2p and Zn2p of fresh and spent catalysts are also shown in Fig. 6B which showed the unchanged oxidation state of Mg and Zn indicating that MgO and ZnO were not reducible at the reaction operating condition.

### 3.1.7. Extended X-ray absorption fine structure (EXAFS)

The EXAFS analysis of fresh and spent catalysts was represented in Fig. 7. Table 4 showed the structural parameters of the 4.8Ni-4.3MgO/ZnO<sup>HT</sup> catalyst fresh and spent catalysts (TOS—100 h, Temp. 800 °C). For the fresh catalyst (Fig. 7a), EXAFS analysis showed the presence of Ni–O bond at a distance of 0.2051 nm with the co-ordination number of 5.77 and a Ni–Zn bond distance of 0.2958 nm with co-ordination number 7.69. The presence of Ni–Zn bond confirmed the direct interaction of Ni with Zn in the catalyst. For the spent catalyst (Fig. 7b), EXAFS analysis only showed the presence of metallic Ni. The Ni–Ni bond distance in the spent catalyst was 0.2483 nm with co-ordination number 7.59. The Ni–Zn bonding was absent for the spent catalyst. Most probably as Ni of NiZn<sub>3</sub> was reduced to metallic Ni (Ni<sup>0</sup>), this Ni–Zn bond was absent (Supporting information Fig. S2). The reduction of nickel species may have weakened the Ni–Zn interaction of NiZn<sub>3</sub> species and the Ni–Zn bond of NiZn<sub>3</sub> species was not detected by EXAFS analysis. But we believe that during the catalysis interaction between Ni and ZnO was present and plays a crucial role for high activity and coke resistant behaviour.

### 3.1.8. O<sub>2</sub>-temperature programmed oxidation (O<sub>2</sub>-TPO)

To find out the coke deposition on the catalyst surface, we carried out O<sub>2</sub>-TPO measurements with the spent 4.8Ni-4.3MgO/ZnO<sup>HT</sup> (TOS—100 h, Temp. 800 °C) catalysts and compared with the O<sub>2</sub>-TPO analysis of the fresh prepared reduced catalyst. O<sub>2</sub>-TPO can be more appropriate to characterise the coke deposited on the catalyst surface during the dry reforming reaction. All the carbonaceous species are combustible by burning with O<sub>2</sub>. The TPO plots are shown in Fig. 8. Table 5 shows the amounts of O<sub>2</sub> consumed during measurements. The TPO profile of the fresh 4.8Ni-4.3MgO/ZnO<sup>HT</sup> catalyst showed an oxygen consumption peak at about 200–400 °C which is due to the oxidation of metallic Ni species (Ni<sup>0</sup>) present in the catalyst, no CO or CO<sub>2</sub> has been evolved as effluent gasses. The TPO profile of spent 4.8Ni-4.3MgO/ZnO<sup>HT</sup> (TOS—100 h, Temp. 800 °C) catalyst also showed similar oxygen consumption peak at 200–500 °C due to the oxidation of metallic Ni. The absence of any peak at higher temperature region confirmed the absence of any carbonaceous species. The

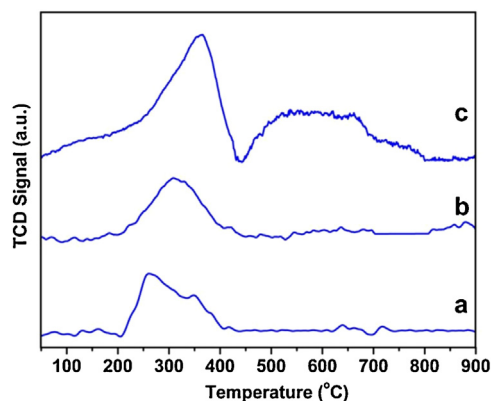


Fig. 8. TPO profiles of (a) fresh 4.8Ni-4.3MgO/ZnO<sup>HT</sup> catalyst (reduced), (b) spent 4.8Ni-4.3MgO/ZnO<sup>HT</sup> catalyst (after 100 h TOS at 800 °C) and (c) Spent 4.7Ni-ZnO<sup>HT</sup> (after 24 h TOS at 800 °C).

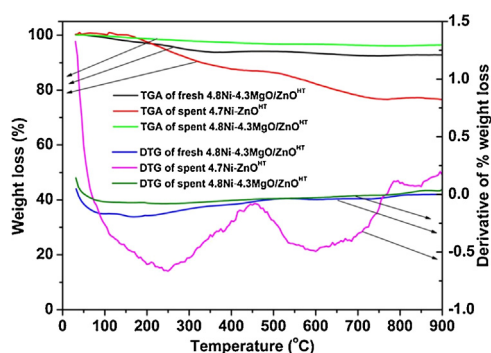
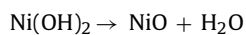


Fig. 9. TGA/DTA plot for the fresh and spent 4.8Ni-4.3MgO/ZnO<sup>HT</sup> catalyst (after 100 h TOS at 800 °C) and spent 4.7Ni-ZnO<sup>HT</sup> (after 24 h TOS at 800 °C).

TPO analysis of spent 4.7Ni-ZnO<sup>HT</sup> (TOS—24 h, Temp. 800 °C) catalyst showed two oxygen consumption peaks at 200–450 °C and 450–800 °C. The first peak was due to the oxidation of metallic Ni species, coke containing hydrogen species and/or surface carbon and the second broad peak at 450–750 °C was due to the combustion of deposited carbon [36] on 4.7Ni-ZnO<sup>HT</sup> catalyst surface after 24 h of time on stream (TOS) reaction, whereas the spent 4.8Ni-4.3MgO/ZnO<sup>HT</sup> (TOS—100 h, Temp. 800 °C) catalyst showed almost no carbon species present on the catalyst surface even after 100 h of TOS reaction. Therefore, the TPO analysis also explained the high coke resisting property of 4.8Ni-4.3MgO/ZnO<sup>HT</sup> catalyst due to the presence of 4.3 wt% MgO.

### 3.1.9. Thermogravimetric (TGA-DTG) analysis

Thermal stability of the fresh 4.8Ni-4.3MgO/ZnO<sup>HT</sup>, spent 4.8Ni-4.3MgO/ZnO<sup>HT</sup> (TOS—100 h, Temp. 800 °C) and spent 4.7Ni-ZnO<sup>HT</sup> (TOS—24 h, Temp. 800 °C) catalysts were investigated by thermogravimetric analysis, in presence of air. Fig. 9 represents the TGA/DTG plot for the catalysts. For fresh catalyst, negligible amount of mass loss was observed during the temperature range between 40–900 °C. The total weight loss (7.5 wt%) was due to the loss of adsorbed water at a temperature range of 40–200 °C and decomposition of Ni(OH)<sub>2</sub> to NiO and H<sub>2</sub>O at about 200–500 °C [70]. As zinc oxide is hygroscopic in nature, it was expected that some amount of water will be adsorbed on the surface of the catalyst.



In the TGA/DTG analysis of the spent catalyst, three separate weight loss region at about 40–200 °C, 200–500 °C and 550–800 °C was noticed. The first weight loss (3 wt%) between temperature 40–200 °C was due to the loss of adsorbed water, the second weight

**Table 4**

EXAFS data of the fresh and spent (TOS – 100 h, Temp. 800 °C) catalysts.

Catalyst	Path	R (10 <sup>-1</sup> nm)	CN	DW (10 <sup>-5</sup> nm <sup>2</sup> )	Δk (10 nm <sup>-1</sup> )	ΔR(10 <sup>-1</sup> nm)	ΔE <sub>0</sub> (eV)	R <sub>f</sub> (%)
4.8Ni-4.3MgO/ZnO <sup>HT</sup> (fresh Catalyst)	Ni–O	2.051 ± 0.011	5.77 ± 0.5	7.0 ± 2.0	3–13	1.0–3.0	–8.4 ± 1.6	1.94
4.8Ni-4.3MgO/ZnO <sup>HT</sup> (spent Catalyst)	Ni–Ni	2.483 ± 0.004	7.59 ± 0.5	5.7 ± 0.4	3–14	1.0–3.0	7.90 ± 0.9	0.34

**Table 5**O<sub>2</sub> consumption during TPO analysis of the catalysts.

Entry	Catalyst	O <sub>2</sub> consumption peaks	O <sub>2</sub> consumption (mmol/g)	Total O <sub>2</sub> consumed (mmol/g)
1	4.8Ni-4.3MgO/ZnO <sup>HT</sup> (Fresh Catalyst)	200–400 °C	0.41555	0.41555
2	4.8Ni-4.3MgO/ZnO <sup>HT</sup> (Spent Catalyst)	200–500 °C	0.42953	0.42953
3	4.7Ni-ZnO <sup>HT</sup> (Spent Catalyst)	200–450 °C 450–800 °C	1.58637 1.51752	3.10389

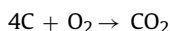
**Table 6**

Catalytic results for different catalysts. For comparison purpose also the pure NiO was listed.

Catalyst	Ni loading (wt%)	Temperature (°C)	CH <sub>4</sub> Conv. (%)	CO <sub>2</sub> Conv. (%)	H <sub>2</sub> /CO ratio
NiO	100	500	0	0	NA
		800	14.3	11.8	NA
Ni-ZnO <sup>ImpCom</sup>	5	500	0	0	NA
		800	20.1	26.4	0.73
Ni-ZnO <sup>Imp</sup>	5	500	0	0	NA
		800	23.7	29.3	0.78
Ni-ZnO <sup>HT</sup>	4.7	500	0	0	NA
		800	96.6	98.1	0.82
Ni-MgO <sup>HT</sup>	4.9	500	0	0	NA
		800	22.3	22.9	0.97
Ni-4.3MgO/ZnO <sup>HT</sup>	2.3	500	3.1	4.2	0.91
		800	98.8	98.9	0.99
Ni-4.3MgO/ZnO <sup>HT</sup>	4.8	500	11.4	13.2	0.88
		800	98.7	98.8	0.99
Ni-4.5MgO/ZnO <sup>HT</sup>	9.2	500	1.1	1.5	0.83
		800	98.6	98.5	0.94
Ni-4.3MgO/ZnO <sup>HT</sup> (O <sub>2</sub> pretreated)	4.8	500	0	0	NA
		800	77.6	65.2	1.12
Ni-4.3MgO/ZnO <sup>HT</sup> (H <sub>2</sub> pretreated)	4.8	500	11.3	13.3	0.89
		800	98.8	98.7	0.99

Reaction condition: Temperature = 500–800 °C, GHSV = 40000 mlg<sup>-1</sup> h<sup>-1</sup>, CH<sub>4</sub>: CO<sub>2</sub>: He (mole ratio) = 1:1:12. NA = Not applicable.

loss (0.5 wt%) between temperature 200–500 °C was due to the decomposition of Ni(OH)<sub>2</sub> to NiO with loss of water and the high temperature weight loss (0.2 wt%) region between temperature 550–800 °C was attributed to the loss of small amount of carbon as carbon dioxide [71]. So from the TG/DTA graph, it was confirmed that almost negligible amount of carbon was deposited on the catalyst surface during 100 h time on stream study. The maximum weight loss of the spent catalyst was due to the loss of water.



We also performed the TGA measurements for the spent 4.7Ni-ZnO<sup>HT</sup> (TOS–24 h, Temp. 800 °C) and compared it with the spent 4.8Ni-4.3MgO/ZnO<sup>HT</sup> (TOS–100 h, Temp. 800 °C) catalyst. Spent 4.7Ni-ZnO<sup>HT</sup> (TOS–24 h, Temp. 800 °C) catalyst showed 13 wt% weight loss in the temperature region 450–800 °C due to the loss of deposited carbon as carbon dioxide, whereas the amount of carbon deposited on the spent 4.8Ni-4.3MgO/ZnO<sup>HT</sup> (TOS–100 h, Temp. 800 °C) catalyst surface was negligible (0.2%). The addition of 4.3 wt% MgO increased the dispersion of Ni and the presence of Ni–ZnO interaction enhanced the coke resistant behaviour of the Ni-MgO/ZnO<sup>HT</sup> catalyst compare to the Ni-ZnO<sup>HT</sup> catalyst.

### 3.1.10. Catalytic Activity

The catalytic activities of prepared catalysts were tested in the temperature range 500–800 °C. The CH<sub>4</sub>: CO<sub>2</sub>: He (mole ratio) feed ratio kept fixed at 1:1:12 at 40000 GHSV (mlg<sup>-1</sup> h<sup>-1</sup>). The activities of the catalysts were tested by changing the wt% of Ni loading and support composition. The activities of different catalysts are shown in Table 6. Pure NiO showed 14.38% of methane and 11.82% of CO<sub>2</sub> conversion but no H<sub>2</sub> formation was observed. Formation of CO and H<sub>2</sub>O was observed at 800 °C. To compare the catalytic activity of Ni–ZnO prepared by the here described method and Ni impregnated on commercial ZnO, the tests were carried out at 500–800 °C. The catalysts were inactive below 500 °C. The Ni impregnated commercial ZnO catalyst (5Ni-ZnO<sup>ImpCom</sup>) showed 20.1% and 26.4% methane and CO<sub>2</sub> conversion with H<sub>2</sub>/CO ratio 0.73 at 800 °C. The observations revealed that RWGS reaction was competing with the Dry reforming reaction. The hydrothermally prepared 4.7Ni-ZnO<sup>HT</sup> catalyst were inactive at 500 °C and showed 96.6%, 98.1% of methane and CO<sub>2</sub> conversion at 800 °C with H<sub>2</sub>/CO ratio 0.82. RWGS over 4.7Ni-ZnO<sup>HT</sup> catalyst were also observed. The results indicated that the prepared ZnO played better role for methane dry reforming compared to Commercial ZnO. The effect of MgO as a support

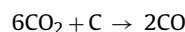
were also tested and it was found that the catalyst was inactive at 500 °C and showed very low methane and CO<sub>2</sub> conversion with 22.3% and 22.9% respectively at 800 °C. The catalytic activities of the catalysts were highly increased when MgO was used as a promoter instead of support. The catalytic activities of Ni-MgO/ZnO<sup>HT</sup> catalysts were investigated and found that 4.8Ni-4.3MgO/ZnO<sup>HT</sup> catalyst showed best activity. It was observed that catalytic activity increased with increasing Ni loading up to 4.8 wt% then again decreased. At 500 °C, 4.8Ni-4.3MgO/ZnO<sup>HT</sup> catalyst showed better activity compared to other two catalysts 2.3Ni-4.3MgO/ZnO<sup>HT</sup>, 9.2Ni-4.5MgO/ZnO<sup>HT</sup>. The catalysts showed almost same high temperature activity with above 98% of methane and CO<sub>2</sub> conversion but H<sub>2</sub>/CO ratio decreased with 9.2 wt% Ni loading. To find out the active species of the catalysts we carried out the catalytic tests with O<sub>2</sub> pretreated catalyst as well as H<sub>2</sub> pretreated catalyst. The catalytic activity of the H<sub>2</sub> pretreated catalyst was found to be better than the O<sub>2</sub> pretreated catalyst. The O<sub>2</sub> pretreated catalyst was inactive at 500 °C. Therefore, metallic Ni was the active species for dry reforming of methane not Ni<sub>x</sub>O<sub>y</sub>. The activity of the fresh non-reduced Ni-MgO/ZnO<sup>HT</sup> catalyst and the reduced catalyst are almost same as shown in Table 6. Although methane has small cracking ability and pure NiO is not catalytically active for the CDRM reaction but methane itself can act as a reducing agent. Monnerat et al. [72], Tanggarnjanavalukul et al. [73], De Vasconcelos et al. [74] reported methane cracking at 400 °C. At our reaction condition all the Ni species will be reduced to metallic Ni which is the active species for the reaction. As both CO and hydrogen are reducing agents, the Ni<sup>0</sup> can not get back to NiO at our reaction condition. At 800 °C, as the space velocity was increased from 10000 to 50,000 ml g<sup>-1</sup> h<sup>-1</sup>, CH<sub>4</sub> and CO<sub>2</sub> conversion was decreased slightly keeping the H<sub>2</sub>/CO ratio almost constant to 1, over the entire space velocity values (Supporting information Fig. S3), using 4.8Ni-4.3MgO/ZnO<sup>HT</sup> catalyst. Turn over frequencies for the reaction at 800 °C was calculated to be  $1.88 \times 10^2 \text{ s}^{-1}$  (with respect to CH<sub>4</sub>) and  $1.90 \times 10^2 \text{ s}^{-1}$  (with respect to CO<sub>2</sub>). The Carbon balance and material balance was also carried out for this catalyst and it was found that the value is in between 98–102%.

## 4. Discussion

### 4.1. Catalytic performance

The effect of support was tested for catalytic activity for dry reforming of methane. The tested materials were NiO, 5Ni-ZnO<sup>ImpCom</sup>, 4.7Ni-ZnO<sup>HT</sup>, 4.9Ni-MgO<sup>HT</sup> and 4.8Ni-4.3MgO/ZnO<sup>HT</sup>. Fig. 10 represents the catalytic activity of different catalysts on methane and CO<sub>2</sub> conversions. Pure NiO showed slight activity at 750 °C. Formation of CO and H<sub>2</sub>O were observed but no H<sub>2</sub> production observed most probably due to RWGS reaction. 4.9Ni-MgO catalyst also showed very low conversion of methane and CO<sub>2</sub> even at 800 °C. It showed only 22.3% and 22.9% of methane and CO<sub>2</sub> conversion respectively. Ni impregnated commercial ZnO (5Ni-ZnO<sup>ImpCom</sup>) also showed very low activity compared to the hydrothermally prepared Ni-ZnO<sup>HT</sup> catalyst. At 800 °C, 5Ni-ZnO<sup>ImpCom</sup> catalyst showed 20.1% and 26.4% of methane and CO<sub>2</sub> conversion respectively whereas hydrothermally prepared 4.7Ni-ZnO<sup>HT</sup> catalyst showed 96.6% and 98.1% of methane and CO<sub>2</sub> conversion respectively. This was due to the dispersion nature of Ni and particle size of 5Ni-ZnO<sup>ImpCom</sup> and 4.7Ni-ZnO<sup>HT</sup> catalysts. Addition of MgO during the hydrothermal preparation method increased the Ni dispersion and reduced the catalyst particle size. Again, presence of metal support interaction enhanced the methane dry reforming activity and coke resistant behaviour of the catalyst. Earlier reports suggested that MgO enhanced the metal dispersion and reduce coke deposition [35,37,38,63–65,75] on the

catalyst surface due to its basic nature. Addition of MgO showed a positive effect on the catalytic activity of the catalyst. 4.7Ni-ZnO<sup>HT</sup> catalyst showed no activity at 500 °C but 4.8Ni-4.3MgO/ZnO<sup>HT</sup> catalyst showed 11.4% and 13.2% of methane and CO<sub>2</sub> conversion respectively. Our results are in agreement with literature where the catalyst particle size also largely influenced the catalytic activity of the catalysts [37,76,77]. The SEM images showed non-uniform catalyst particle sizes of 5Ni-ZnO<sup>ImpCom</sup> catalyst whereas hydrothermally prepared 4.7Ni-4.3MgO-ZnO<sup>HT</sup> catalyst showed almost uniform particle size which increased the catalytic activity of the catalyst. Presence of a basic support like MgO in 4.8Ni-4.3MgO/ZnO<sup>HT</sup> catalyst increased metal dispersion which improved the catalytic activity. In addition, MgO reduced the acidity of the catalyst by decreasing surface acidic sites which were responsible for carbon accumulation [37,38,56–65,75,78]. The low methane conversion and high CO<sub>2</sub> conversion over 4.7Ni-ZnO<sup>HT</sup> compared to 4.8Ni-4.3MgO/ZnO<sup>HT</sup> catalyst was observed and this is due to the prominent side reactions like boudouard reaction and RWGS reaction. The addition of small amount of MgO inhibited the competing reactions, carbon deposition over the catalyst surface and highly raised the activity of the catalyst [39,78]. TGA analysis showed that over 4.7Ni-ZnO<sup>HT</sup> catalyst, substantial amount of carbon (13 wt%) was deposited only after 18 h of time on stream reaction whereas over 4.8Ni-4.3MgO/ZnO<sup>HT</sup> catalyst, only 0.2 wt% of carbon deposition took place after 100 h. Presence of MgO in 4.8Ni-4.3MgO/ZnO<sup>HT</sup> catalyst increased the chemisorptions and dissociation of CO<sub>2</sub> and accelerated Carbon elimination by the following reaction [1,79].



To optimize the Ni loading of the catalyst, the catalytic activity of the Ni-MgO/ZnO<sup>HT</sup> catalysts with different wt% of Ni-loading was examined at temperature range 500–800 °C for carbon dioxide reforming of methane. The catalytic activities of 2.3Ni-4.3MgO/ZnO<sup>HT</sup>, 4.8Ni-4.3MgO/ZnO<sup>HT</sup> and 9.2Ni-4.5MgO/ZnO<sup>HT</sup> catalysts are shown in Fig. 11. 4.8Ni-4.3MgO/ZnO<sup>HT</sup> catalyst showed better catalytic activity compared to the other two catalysts. The catalytic activity of these catalysts was governed by the factors like wt% of Ni loading, catalyst particle size and their reducible nature. For carbon dioxide reforming of methane, 2.3Ni-4.3MgO/ZnO<sup>HT</sup> and 9.2Ni-4.5MgO/ZnO<sup>HT</sup> catalysts showed very low activities at 500 °C with 3.1%, 1.1% methane and 4.2%, 1.5% CO<sub>2</sub> conversion respectively, whereas 4.8Ni-4.3MgO/ZnO<sup>HT</sup> catalyst initialized the reaction at 500 °C with 11.4% methane and 13.2% CO<sub>2</sub> conversion. From H<sub>2</sub>-chemisorption measurement it was observed that Ni particle size was increasing with increasing wt% of Ni loading (Supporting information Table S1). 2.3Ni-4.3MgO/ZnO<sup>HT</sup>, 4.8Ni-4.3MgO/ZnO<sup>HT</sup> and 9.2Ni-4.5MgO/ZnO<sup>HT</sup> catalyst has Ni particle size 5.2 nm, 5.7 nm and 12.3 nm respectively. H<sub>2</sub>-TPR profiles showed much easily reducible NiO species in 2.3Ni-4.3MgO/ZnO<sup>HT</sup>, 4.8Ni-4.3MgO/ZnO<sup>HT</sup> catalysts whereas 9.2Ni-4.5MgO/ZnO<sup>HT</sup> catalyst showed hardly reducible NiO species. The easily reducible NiO species with smaller particle sizes showed better catalytic activity [80]. The lower activity of 2.3Ni-4.3MgO/ZnO<sup>HT</sup> catalyst was due to the lower loading of Ni which provides less number of active sites for the reaction to take place. The low activity of 9.2Ni-4.5MgO/ZnO<sup>HT</sup> catalyst was due to the higher loading of Ni which led to formation of much bigger Ni particles, lowering the activity. The hardly reducible NiO particles were also a reason for low catalytic activity of 9.2Ni-4.5MgO/ZnO<sup>HT</sup> catalyst.

Oyama et al. reported that reverse water gas shift (RWGS) reaction is the main problem for the methane dry reforming reaction, as with increasing pressure; the valuable hydrogen gets consumed by RWGS reaction [18]. But at atmospheric pressure, using a suitable catalyst it is possible to convert two major greenhouse gases

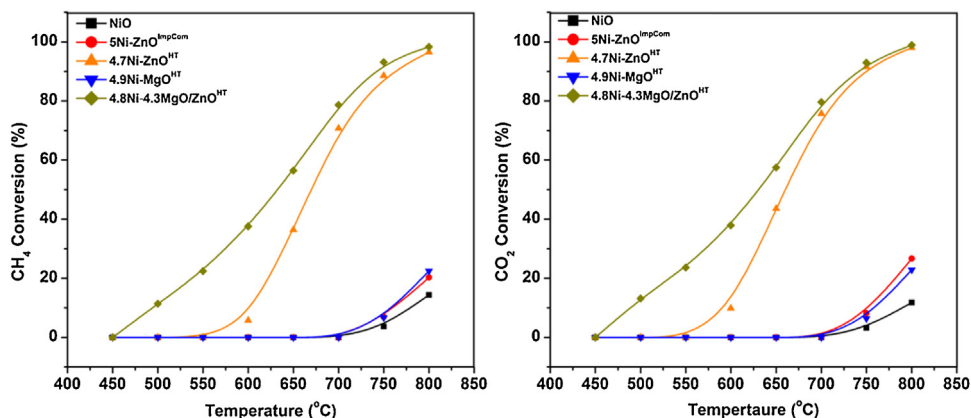


**Fig. 10.** Effect of support on the activity of the catalyst. Reaction Condition: reaction time (6 h),  $\text{CH}_4$ :  $\text{CO}_2$ : He = 1:1:12 (feed ratio), GHSV ( $40000 \text{ ml g}^{-1} \text{ h}^{-1}$ ), pressure (1 atm).

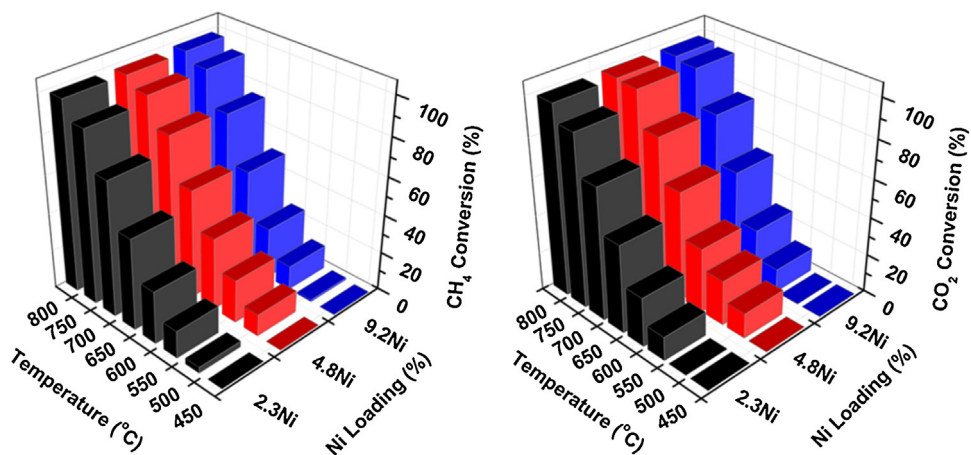


**Fig. 11.** Effect of Ni loading on the conversions of reactants. Reaction Condition: reaction time (6 h), Catalyst ( $4.8\text{Ni}-4.3\text{MgO}/\text{ZnO}^{\text{HT}}$ ),  $\text{CH}_4$ :  $\text{CO}_2$ : He = 1:1:12 (feed ratio), GHSV ( $40000 \text{ ml g}^{-1} \text{ h}^{-1}$ ), pressure (1 atm).

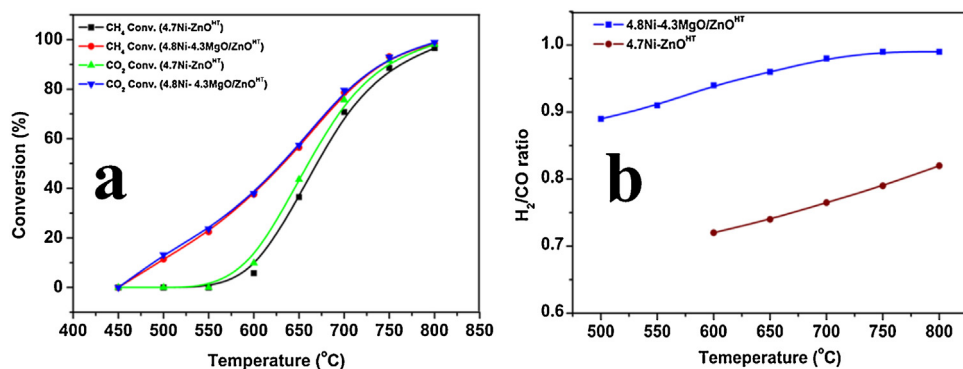


**Fig. 12.** The activities of prepared  $4.7\text{Ni}-\text{ZnO}^{\text{HT}}$  and  $4.8\text{Ni}-4.3\text{MgO}/\text{ZnO}^{\text{HT}}$  catalysts. Reaction Condition: reaction time (6 h),  $\text{CH}_4$ :  $\text{CO}_2$ : He = 1:1:12 (feed ratio), GHSV ( $40000 \text{ ml g}^{-1} \text{ h}^{-1}$ ), pressure (1 atm).

(methane and  $\text{CO}_2$ ) to synthesis gas with  $\text{H}_2/\text{CO}$  ratio 1 and the produced synthesis gas can be utilized by gas to liquid (GTL) process. The activities of prepared  $4.7\text{Ni}-\text{ZnO}^{\text{HT}}$  and  $4.8\text{Ni}-4.3\text{MgO}/\text{ZnO}^{\text{HT}}$  catalysts for  $\text{CO}_2$  reforming of methane using  $\text{CO}_2$  to  $\text{CH}_4$  ratio 1, was carried out over the temperature range  $500\text{--}800^\circ\text{C}$  and space velocity of  $40000 \text{ ml g}^{-1} \text{ h}^{-1}$  (Fig. 12). The equilibrium conversion was also calculated and compared (Supporting information Fig. S4). The conversion of methane was increased with increasing temperature due decomposition of methane ( $\text{CH}_4 \rightarrow \text{C} + 2\text{H}_2$ ) at higher temperatures. It was also observed that at lower temperature, the  $\text{H}_2/\text{CO}$  ratio was less than 1 (Fig. 12b). This may be due to the reverse

water gas shift (RWGS) reaction ( $\text{CO}_2 + \text{H}_2 \rightarrow \text{CO} + \text{H}_2\text{O}$ ). RWGS was favourable at lower temperature where methane conversion was lower at atmospheric pressure. Our results are in consistent with the previous reports where researchers have found that at higher temperature methane conversion is higher leading to  $\text{H}_2/\text{CO}$  ratio to 1 [37]. At higher reaction temperature (above  $650^\circ\text{C}$ ), the RWGS activity decreases and  $\text{H}_2/\text{CO}$  ratio became 1. At higher temperature under equilibrium condition, both RWGS and  $\text{CH}_4$  decomposition compensate each other to maintain  $\text{CH}_4$  and  $\text{CO}_2$  conversion almost similar with  $\text{H}_2/\text{CO}$  ratio almost 1. Therefore, the reactant conversion and  $\text{H}_2/\text{CO}$  ratio clearly indicated that the RWGS reaction

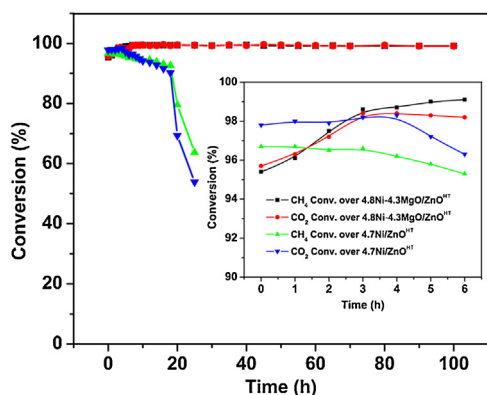
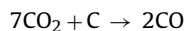


**Fig. 13.** Effect of Time on Stream on the activity of the catalyst. Reaction Condition: temperature (800 °C), CH<sub>4</sub>: CO<sub>2</sub>: He = 1:1:12 (feed ratio), GHSV (40000 mlg<sup>-1</sup> h<sup>-1</sup>), pressure (1 atm).

was minimized and methane dry reforming was the main reaction during the catalytic process over 4.8Ni-4.3MgO/ZnO<sup>HT</sup> catalyst. If RWGS reaction was dominant over methane dry reforming reaction, CO<sub>2</sub> conversion would have been much more higher compared to methane with H<sub>2</sub>/CO less than 1, which indeed was the case for the 4.7Ni-ZnO<sup>HT</sup> catalyst but not for 4.8Ni-4.3MgO/ZnO<sup>HT</sup> catalyst. Addition of MgO minimized the RWGS reaction. We also carried out RWGS reaction over 4.8Ni-4.3MgO/ZnO<sup>HT</sup> catalyst and found that CO<sub>2</sub> conversion was very low compared to the equilibrium conversion (Supporting information Fig. S5).

The catalytic stability of 4.7Ni-ZnO<sup>HT</sup> and 4.8Ni-4.3MgO/ZnO<sup>HT</sup> catalysts was studied at 800 °C and is shown in Fig. 13. Although, the initial activity for both the catalyst was same but 4.7Ni-ZnO<sup>HT</sup> catalyst started deactivating continuously with time on stream and the activity was decreased from 96.7% to 63.7% (CH<sub>4</sub> conversion) after 24 h of time on stream. On the contrary 4.8Ni-4.3MgO/ZnO<sup>HT</sup> catalyst showed very high stability without any deactivation up to 100 h time on stream. In general, Ni-supported catalyst deactivation takes place easily due to carbon deposition over the active Ni sites either by boudouard reaction (2CO → CO<sub>2</sub> + C) or by methane decomposition (CH<sub>4</sub> → C + 2H<sub>2</sub>) [42]. There is also a possibility of coke deposition due to the reduction of CO by hydrogen (CO + H<sub>2</sub> → C + H<sub>2</sub>O). The presence of MgO increased the Ni dispersion over ZnO support and Ni also showed interaction with ZnO (as evidenced by H<sub>2</sub>-TPR and EXAFS). This might have been reduced the coke deposition [8,81]. Additionally, the presence of MgO decreased the size of the Ni nanoparticles (<10 nm), which is the advantage against sintering at high temperatures in presence of hydrogen, produced during dry reforming reaction. We also believe that due to basic nature of MgO, the CO<sub>2</sub> adsorption behaviour of Ni-MgO/ZnO<sup>HT</sup> was increased compared to the Ni-ZnO<sup>HT</sup> catalyst. Also, due to the presence of MgO, the dissociation behaviour of CO<sub>2</sub> and coke removal process was increased [1,82] (Supporting information Fig. S6) by the following reaction:



From the CO<sub>2</sub>-TPD results it can be seen that most of the CO<sub>2</sub> gets desorbed below 550 °C but not all. The catalyst contains only 4.3% MgO and the 4.8Ni-4.3MgO/ZnO<sup>HT</sup> catalyst has slightly higher basicity than 4.7Ni-ZnO<sup>HT</sup> catalyst. It can be seen from the CO<sub>2</sub>-TPD results that a small amount of CO<sub>2</sub> also get desorbed at above 550 °C (between 550–700 °C) indicating the increase in strong basic sites. First, MgO increased the Ni dispersion which in turn reduced the tendency of coking due to smaller size of nickel of 4.8Ni-4.3MgO/ZnO<sup>HT</sup> catalyst compared to 4.7Ni-ZnO<sup>HT</sup> catalyst, as it is also reported that the smaller size of nickel are far more coke resistant than the larger nickel particles [35,36,46,80,83]. So, the coke

resistant behaviour of 4.8Ni-4.3MgO/ZnO<sup>HT</sup> catalyst is the reason behind the better activity compared to the activity of 4.7Ni-ZnO<sup>HT</sup> catalyst. But we can't exclude the fractional contribution of MgO at higher temperature (550–700 °C). The stability of the catalyst was tested at 800 °C. So, higher dispersion of nickel after addition of MgO, reduced coking and is the most likely reason for the catalysts longtime stability.

We also calculated the Mass and Heat transfer limitation for CO<sub>2</sub> reforming of methane over 4.8Ni-4.3MgO/ZnO<sup>HT</sup> catalyst using Weisz-Prater and Mears criterion (Supporting information).

Applying Weisz-Prater criterion with respect to methane (conversion 11.5%)

$$C_{WP} = \frac{-r'_A(\text{obs})\rho_c R^2}{D_e C_{As}} < 1$$

The  $C_{WP}$  value was obtained  $3.88 \times 10^{-1}$  which is less <1, indicated that there was no internal diffusion for 4.8Ni-4.3MgO/ZnO<sup>HT</sup> catalyst [35,75].

Applying Mears criterion with respect to CO<sub>2</sub> (conversion 13.2%)

$$\left| \frac{-\Delta H_r(-r'_A)\rho_b RE}{h_t T_b^2 R_g} \right| < 0.15$$

The value obtained was  $1.29 \times 10^{-4}$ , which is <0.15, indicated that there was no external interphase heat transfer for 4.8Ni-4.3MgO/ZnO<sup>HT</sup> catalyst.

#### 4.2. Kinetics of the reaction

In order to carry out a more accurate kinetic analysis, the experiments were carried out at a reaction condition at which heat and mass transfer limitations can be neglected. The effect of partial pressures of different reactants on methane and CO<sub>2</sub> consumption rates are depicted in Fig. 14. The study was carried out over 4.8Ni-4.3MgO/ZnO<sup>HT</sup> catalyst (pre-reduced) at atmospheric pressure at the temperature range 480–520 °C. Heat and mass transfer limitations for dry reforming of methane over 4.8Ni-4.3MgO/ZnO<sup>HT</sup> catalyst was carried out by Weisz-Prater and Mears analysis (Supporting information) [75]. Again the transport limitations were ruled out by dilution of the catalyst with inert material. The change in conversion of methane and CO<sub>2</sub> with the pellet size and GHSV was negligible (Supporting information Fig. S7) [84]. The Mears Criterion for External (Interphase) Heat Transfer for methane and CO<sub>2</sub> was found to be  $1.29 \times 10^{-4}$  and  $0.88 \times 10^{-4}$  respectively (<0.15). To get an insight into the kinetics of the methane dry reforming reaction, we have calculated the rate of the reaction by continuity equation for the reference component.

$$r_{\text{CO}} = -r_A = dX_A/d(W_{\text{cat}}/F_A)$$

$r_A$  = reaction rate with respect to component A,  $X_A$  = conversion of the reactant A,  $W_{\text{cat}}$  = weight of the catalyst used,  $F_A$  = flow of the reactant A.

Reaction rate was also a function of partial pressures of different reactants of the reaction. For dry reforming of methane the power rate law expression can be written as follows.

$$-r_{\text{CH}_4} = k_1 \cdot (P_{\text{CH}_4})^{m_1} \cdot (P_{\text{CO}_2})^{n_1} \quad (1)$$

$$-r_{\text{CO}_2} = k_2 \cdot (P_{\text{CH}_4})^{m_2} \cdot (P_{\text{CO}_2})^{n_2} \quad (2)$$

where  $k_1$ ,  $k_2$ ,  $m_1$ ,  $m_2$ ,  $n_1$  and  $n_2$  are the unknown parameters to be determined.

The experiments were done over 4.8Ni-4.3MgO/ZnO<sup>HT</sup> catalyst by changing the partial pressure of the reactants. The measurements were carried out keeping the partial pressure of one reactant constant, where the partial pressure of the other reactant varied

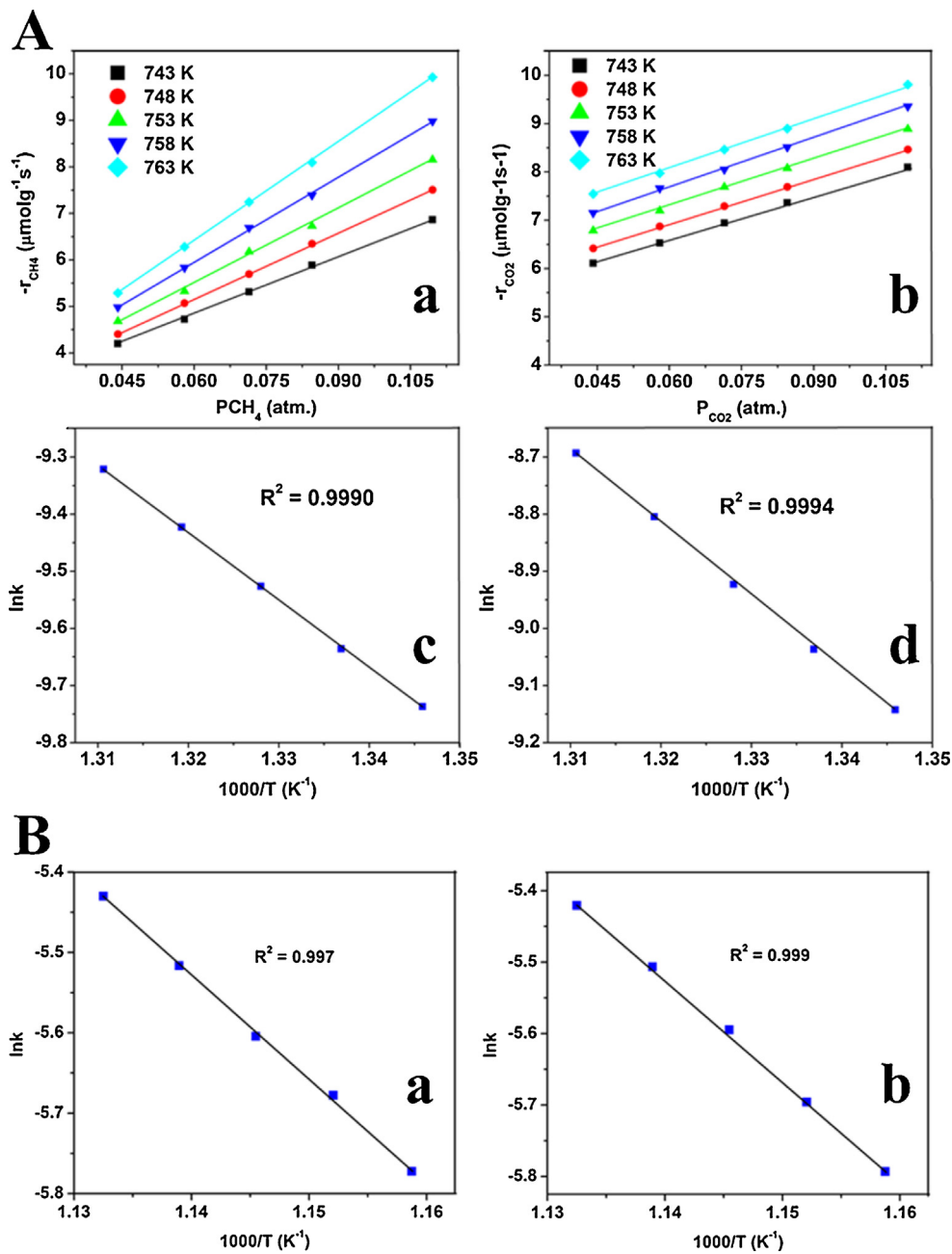


**Fig. 14.** A Changes in reaction rates with changes in partial pressure of (a) CH<sub>4</sub>, (b) CO<sub>2</sub> at indicated temperatures and Arrhenius plots of  $\ln k$  vs  $1000/T$  for (c) CH<sub>4</sub> and (d) CO<sub>2</sub> activation energies over .8Ni-4.3MgO/ZnO<sup>HT</sup> catalyst and B. Arrhenius plots of  $\ln k$  vs  $1000/T$  for (c) CH<sub>4</sub> and (d) CO<sub>2</sub> activation energies over 4.7Ni-ZnO<sup>HT</sup> catalyst. Reaction Condition: temperature (490–510 °C), CH<sub>4</sub>: CO<sub>2</sub>: He = 1:1:12 (feed ratio), GHSV (40,000 ml g<sup>-1</sup> h<sup>-1</sup>), pressure (1 atm).

**Table 7**  
The parameters used for the plots shown in Fig. 14.

Temperature (K)	$-r_{CH_4} = k_1 \times (P_{CH_4})^{m_1} \times (P_{CO_2})^{n_1}$			$-r_{CO_2} = k_2 \times (P_{CH_4})^{m_2} \times (P_{CO_2})^{n_2}$		
	$k_1$	$m_1$	$n_1$	$k_2$	$m_2$	$n_2$
For 4.7Ni-ZnO <sup>HT</sup> catalyst						
863	$3.11 \times 10^{-3}$	0.97	0.11	$3.05 \times 10^{-3}$	0.88	0.009
868	$3.36 \times 10^{-3}$	0.95	0.12	$3.36 \times 10^{-3}$	0.87	0.02
873	$3.68 \times 10^{-3}$	0.92	0.13	$3.72 \times 10^{-3}$	0.86	0.05
878	$4.06 \times 10^{-3}$	0.89	0.15	$4.06 \times 10^{-3}$	0.85	0.08
883	$4.38 \times 10^{-3}$	0.86	0.16	$4.51 \times 10^{-3}$	0.83	0.11
For 4.8Ni-4.3MgO/ZnO <sup>HT</sup> catalyst						
743	$5.91 \times 10^{-5}$	0.92	0.36	$1.06 \times 10^{-4}$	0.76	0.20
748	$6.53 \times 10^{-5}$	0.89	0.39	$1.19 \times 10^{-4}$	0.73	0.22
753	$7.29 \times 10^{-5}$	0.87	0.41	$1.33 \times 10^{-4}$	0.71	0.23
758	$8.08 \times 10^{-5}$	0.85	0.42	$1.50 \times 10^{-4}$	0.69	0.24
763	$8.95 \times 10^{-5}$	0.84	0.44	$1.68 \times 10^{-4}$	0.68	0.25

at the temperature range. The plots were drawn by taking five points, which showed almost linear trend with increasing rate, with increasing temperature. The kinetic parameters are given in Table 7, showed that the partial pressure of  $P_{CH_4}$  had stronger influence on the rate of the reaction compared to  $P_{CO_2}$ . The results indicated the lower reaction order for  $CO_2$  as compared to methane [85]. From the literature reports it is very clear that the reaction kinetics is dependent on the surface properties of the catalysts. Different activation energies for the same reactants and reaction kinetics for the same dry reforming of methane reaction have been observed and reported by different researchers. Wei and Iglesia [84] reported (Ni–MgO) that the C–H bond cleavage is the rate determining step of dry reforming of methane and the rate is independent of partial pressure of  $CO_2$ , whereas Múnera et al. [85] reported (Rh– $La_2O_3$ ) that partial pressure of methane has stronger influence on reaction rate, but they did not rule out the contribution from the co-reactant  $CO_2$ . Múnera et al. [85] reported that both decomposition and the oxygenation of the carbon species are slower steps and the heat and mass transfer limitations were negligible in their case. Pakhare et al. [86] reported (Rh– $La_2Zr_2O_7$ ) the dual site mechanism, where methane and  $CO_2$  activated at different sites. Two models, one in which  $CH_4$  activation is rate determining and in another,  $CO_2$  activation is rate determining. Addition of basic promoter increased the  $CO_2$  activation rates. They also reported that the higher activation energy of methane indicated that methane activation is the slower step. So, from their observation it is clear that the kinetics was dependent on the type of catalyst active sites. Zhang et al. (Rh supported  $YSZ$ ,  $Al_2O_3$ ,  $TiO_2$ ,  $SiO_2$ ,  $La_2O_3$ , MgO) [42] and O'Connor et al. (Pt/ $ZrO_2$ , Pt/ $Al_2O_3$ ) [87] reported that  $CO_2$  dissociation and the surface carbon oxidation is the slowest step in DRM. Some of the reports also described that the rate of DRM reaction depends mainly on methane decomposition and fractionally on  $CO_2$  [85,88–92]. Das et al. [92] actually reported that the influence of  $CO_2$  partial pressure is higher than the partial pressure of methane on the reaction rate. On the basis of these literature reports, we have done a comparative analysis for the reaction kinetics of  $4.7Ni-ZnO^{HT}$  and  $4.8Ni-4.3MgO/ZnO^{HT}$  catalyst to find out the effect of addition of MgO on the reaction kinetics. The analysis showed that the addition of MgO increased the rate dependence on the partial pressure of  $CO_2$  [86] but the influence of the partial pressure of methane on the reaction kinetics was major. The kinetics was not solely dependent on the methane activation but fractional dependence on the partial pressure of  $CO_2$  was also observed and it was also reported by earlier literature reports [85,88–92].

The kinetic parameters were obtained by Polymath 5.1 software. The reaction rates with the change in partial pressure of methane and  $CO_2$  are represented in Fig. 14a and 14b. Calculations were done at methane and  $CO_2$  conversion below 10%. Rate of methane conversion was governed by the Eq. (1) and that of  $CO_2$  conversion was governed by Eq. (2). The Arrhenius model was applied for the estimation of activation energy for methane (Fig. 14Ac) and  $CO_2$  (Fig. 14Ad) in dry reforming of methane over  $4.8Ni-4.3MgO/ZnO^{HT}$  catalyst. The activation energy for methane and  $CO_2$  were 97.4 kJ/mol and 106.3 kJ/mol. We have also calculated the activation energies of methane and  $CO_2$  over  $4.7Ni-ZnO^{HT}$  catalyst and found that the activation energies are 110.7 kJ/mol (Fig. 14Ba) and 118.4 kJ/mol (Fig. 14Bb) for methane and  $CO_2$  respectively. The lower value of activation energy over  $4.8Ni-4.3MgO/ZnO^{HT}$  catalyst corresponds to the highly dispersed Ni supported on MgO modified ZnO support with the presence of metal support interaction.

## 5. Conclusion

Ni nanoparticles supported on MgO promoted ZnO catalyst was prepared by hydrothermal method. The catalyst was found to be

very active for reforming of methane with carbon dioxide without any deactivation till 100 h time on stream. The presence of MgO increases the dispersion of Ni and the size of the Ni-nanoparticles decreases compare to the catalyst where MgO was not present. The presence of metal support interaction was evidenced by  $H_2$ -TPR and EXAFS analysis. Heat and mass transfer calculation showed that the catalyst does not show any heat and mass transfer during the  $CO_2$  reforming of methane. The kinetic analysis also showed that the activation energy for methane and  $CO_2$  were 97.4 kJ/mol and 106.3 kJ/mol respectively, which is very low over Ni–MgO/ZnO catalyst due to the presence of highly dispersed Ni nanoparticles and metal support interaction which also enhanced the coke resistant behavior of the Ni–MgO/ZnO catalyst.

## Acknowledgements

R.S. thanks UGC, New Delhi, India for their fellowships. R.B. thanks CSIR for funding in the form of Network Project (CSC-0125, CSC-0117) and DST for funding in the form of AISRF Grand Challenge Project (DST/INT/Aus/GCP-4/13(C)). The Director, CSIR-IIP, was acknowledged for his help and encouragement. The authors thank the Analytical Science Division, Indian Institute of Petroleum for analytical services. The XAFS measurements were performed at KEK-IMSS-PF, Tsukuba, Japan with the approval of Proton Factory Advisory Committee (Project 2013G210 and 2014G070).

## Appendix A. Supplementary data

Supplementary data associated with this article can be found, in the online version, at <http://dx.doi.org/10.1016/j.apcatb.2016.03.029>.

## References

- [1] R. Bouarab, O. Cherifi, A. Auroux, *Green Chem.* 5 (2003) 209–212.
- [2] K.S. Jung, B.Y. Coh, H.I. Lee, *Bull. Korean Chem. Soc.* 20 (1999) 89–94.
- [3] T. Wurzel, S. Malcus, L. Mieczko, *Chem. Eng. Sci.* 55 (2000) 3955–3966.
- [4] H.Y. Wang, E. Ruckenstein, *Appl. Catal. A: Gen.* 204 (2000) 143–152.
- [5] J.Z. Luo, Z.L. Yu, C.F. Ng, C.T. Au, *J. Catal.* 194 (2000) 198–210.
- [6] S. Tang, L. Ji, H.C. Zeng, K.L. Tan, K. Li, *J. Catal.* 194 (2000) 424–430.
- [7] J.H. Edwards, A.M. Maitra, *Fuel Process. Technol.* 42 (1995) 269–289.
- [8] M.C.J. Bradford, M.A. Vannice, *Catal. Rev.* 41 (1999) 1–42.
- [9] F. Solymosi, G. Kutsán, A. Erd'ohelyi, *Catal. Lett.* 11 (1991) 149–156.
- [10] A. Erd'ohelyi, J. Cserényi, F. Solymosi, *J. Catal.* 141 (1993) 287–299.
- [11] J. Wei, E. Iglesia, *J. Catal.* 225 (2004) 116–127.
- [12] A. Erd'ohelyi, K. Fodor, T. Szailer, *Appl. Catal. B: Environ.* 53 (2004) 153–160.
- [13] M. Ghelamallah, P. Granger, *Fuel* 97 (2012) 269–276.
- [14] Z. Hou, P. Chen, H. Fang, X. Zheng, T. Yashima, *Int. J. Hydrogen Energy* 31 (2006) 555–561.
- [15] S. Ozkara-Aydinoglu, E. Ozensoy, A.E. Aksoy, *Int. J. Hydrogen Energy* 34 (2009) 9711–9722.
- [16] S. Ozkara-Aydinoglu, A.E. Aksoy, *Int. J. Hydrogen Energy* 36 (2011) 2950–2959.
- [17] M.A. Soria, C. Mateos-Pedrero, A. Guerrero-Ruiz, I. Rodríguez-Ramos, *Int. J. Hydrogen Energy* 36 (2011) 15212–15220.
- [18] S.T. Oyama, P. Hacırlıoglu, Y. Gub, D. Lee, *Int. J. Hydrogen Energy* 37 (2012) 10444–10450.
- [19] J. Zhang, H. Wang, A.K. Dalai, *J. Catal.* 249 (2007) 300–310.
- [20] F. Mirzaei, M. Rezaei, F. Meshkini, *Chem. Eng. Tech.* 37 (6) (2014) 973–978.
- [21] A.I. Paksoy, B.S. Caglayan, A.E. Aksoy, *Appl. Catal. B: Environ.* 168 (2015) 164–174.
- [22] M. Yu, Y.A. Zhu, Y. Lu, G. Tong, K. Zhu, X. Zhou, *Appl. Catal. B: Environ.* 165 (2015) 43–56.
- [23] Z. Li, L. Mo, Y. Kathiraser, S. Kawi, *ACS Catal.* 4 (2014) 1526–1536.
- [24] R. Zanganeh, M. Rezaei, A. Zamaniyan, *Int. J. Hydrogen Energy* 38 (2013) 3012–3018.
- [25] F. Solymosi, G. Kutsán, A. Erd'ohelyi, *Catal. Lett.* 11 (1991) 149–156.
- [26] A. Erd'ohelyi, J. Cserényi, F. Solymosi, *J. Catal.* 141 (1993) 287–299.
- [27] A. Erd'ohelyi, K. Fodor, T. Szailer, *Appl. Catal. B: Environ.* 53 (2004) 153–160.
- [28] M.C.J. Bradford, M.A. Vannice, *J. Catal.* 173 (1998) 157–171.
- [29] S. Tang, J. Lin, K.L. Tan, *Catal. Lett.* 59 (1999) 129–135.
- [30] X. Li, J.S. Chang, S.E. Park, *React. Kinet. Catal. Lett.* 67 (2) (1999) 375–381.
- [31] A.J. Brungs, A.P.E. York, J.B. Claridge, C.M. Alvarez, M.L.H. Green, *Catal. Lett.* 70 (2000) 117–122.
- [32] D. Li, Y. Nakagawa, K. Tomishige, *Appl. Catal. A: Gen.* 408 (2011) 1–24.
- [33] T. Osaki, T. Mori, *J. Catal.* 204 (2001) 89–97.

- [34] L. Kepinski, B. Stasinska, T. Borowiecki, *Carbon* 38 (2000) 1845–1856.
- [35] S. Zhang, S. Muratsugu, N. Ishiguro, M. Tada, *ACS Catal.* 3 (2013) 1855–1864.
- [36] A. Djaidja, S. Libs, A. Kiennemann, A. Barama, *Catal. Today* 113 (2006) 194–200.
- [37] L. Pino, A. Vita, F. Cipitì, M. Laganà, V. Recupero, *Appl. Catal. B: Environ.* 104 (2011) 64–73.
- [38] A. Shamsi, *Appl. Catal. A: Gen.* 277 (2004) 23–30.
- [39] K. Nagaoka, M. Okamura, K. Aika, *Catal. Commun.* 2 (2001) 255–260.
- [40] M. García-Diéguez, I.S. Pieta, M.C. Herrera, M.A. Larrubia, L.J. Alemany, *J. Catal.* 270 (2010) 136–145.
- [41] T. Sodesawa, A. Dobashi, F. Nozaki, *React. Kinet. Catal. Lett.* 12 (1979) 107–111.
- [42] Z.L. Zhang, Z.A. Tsiourari, A.M. Efstathiou, X.E. Verykios, *J. Catal.* 158 (1996) 51–63.
- [43] A.T. Ashcroft, A.K. Cheetham, M.L.H. Green, P.D.F. Vernon, *Nature* 352 (1991) 225–226.
- [44] J.T. Richardson, S.A. Paripatyadar, *Appl. Catal. A: Gen.* 61 (1990) 293–309.
- [45] S.M. Stagg, E. Romeo, C. Padro, D.E. Resasco, *J. Catal.* 178 (1998) 137–145.
- [46] J.H. Bitter, K. Seshan, J.A. Lercher, *J. Catal.* 183 (1999) 336–343.
- [47] S. Ghosh, S.S. Acharyya, R. Tiwari, B. Sarkar, R.K. Singha, C. Pendem, T. Sasaki, R. Bal, *ACS Catal.* 4 (2014) 2169–2174.
- [48] S.S. Acharyya, S. Ghosh, R. Tiwari, C. Pendem, T. Sasaki, R. Bal, *ACS Catal.* 5 (2015) 2850–2858.
- [49] S.S. Acharyya, S. Ghosh, R. Bal, *ACS Appl. Mater. Interfaces* 6 (2014) 14451–14459.
- [50] S. Ghosh, S.S. Acharyya, T. Sasaki, R. Bal, *Green Chem.* 17 (2015) 1867–1876.
- [51] S.S. Acharyya, S. Ghosh, R. Bal, *Chem. Commun.* 51 (2015) 5998–6001.
- [52] A. Shukla, R.K. Singha, T. Sasaki, R. Bal, *Green Chem.* 17 (2015) 785–790.
- [53] E.A. Stern, M. Newvill, B. Ravel, Y. Yacoby, D. Haskel, *Physica B* 208 (1995) 117–120.
- [54] M. Newvill, P. Livins, Y. Yacoby, E.A. Stern, J.J. Rehr, *Phys. Rev. B: Condens. Matter* 47 (1993) 14126–14131.
- [55] A.L. Aukudinov, B. Ravel, J.J. Rehr, S.D. Conradson, *Phys. Rev. B: Condens. Matter* 58 (1998) 7565–7576.
- [56] A.L. Ankudinov, A.I. Nesvizhskii, J.J. Rehr, *Phys. Rev. B: Condens. Matter* 67 (2003) 1151201–1151206.
- [57] V. Tiwari, J. Jiang, V. Sethi, P. Bisi, *Appl. Catal. A: Gen.* 345 (2008) 241–246.
- [58] Y.J.O. Asencios, J.D.A. Bellido, E.M. Assaf, *Appl. Catal. A: Gen.* 397 (2011) 138–144.
- [59] H. Jiang, H. Li, H. Xu, Y. Zhang, *Fuel Process Technol.* 88 (2007) 988–995.
- [60] R.K. Marella, C.K.P. Neeli, S.R.R. Kamaraju, D.R. Burri, *Catal. Sci. Technol.* 2 (2012) 1833–1838.
- [61] I. Melián-Cabrera, M.L. Granados, J.L.G. Fierro, *J. Catal.* 210 (2002) 273–284.
- [62] C. Song, W. Pan, *Catal. Today* 98 (2004) 463–484.
- [63] J. Zieliński, *J. Catal.* 76 (1982) 157–163.
- [64] A. Ballarín, F. Basile, P. Benito, I. Bersani, G. Fornasari, S. de Miguel, S.C.P. Maina, J. Vilella, A. Vaccari, O.A. Scelz, *Appl. Catal. A: Gen.* 433–434 (2012) 1–11.
- [65] G. Xu, K. Shi, Y. Gao, H. Xu, Y. Wei, *J. Mol. Catal. A Chem.* 147 (1999) 47–54.
- [66] T. Horiuchi, K. Sakuma, T. Fukui, Y. Kubo, T. Osaki, T. Mori, *Appl. Catal. A: Gen.* 144 (1996) 111–120.
- [67] S. Wang, G.Q. (Max) Lu, *J. Chem. Technol. Biotechnol.* 75 (2000) 589–595.
- [68] V.R. Choudhary, B.S. Uphade, A.S. Mammam, *Appl. Catal. A: Gen.* 168 (1998) 33–46.
- [69] L. Xiancai, W. Min, L. Zhihua, H. Fei, *Appl. Catal. A: Gen.* 290 (2005) 81–86.
- [70] X. Li, S. Xiong, J. Li, J. Bai, Y. Qian, *J. Mater. Chem.* 22 (2012) 14276–14283.
- [71] B. Barros, D. Melo, S. Libs, A. Kiennemann, *Appl. Catal. A: Gen.* 378 (2010) 69–75.
- [72] B. Monnerat, L. Kiwi-Minsker, A. Renken, *Chem. Eng. Sci.* 56 (2001) 633–639.
- [73] C. Tanggarnjanavalukul, W. Donphai, T. Wittoon, M. Chareonpanich, J. Limtrakul, *Chem. Eng. J.* 262 (2015) 364–371.
- [74] B.R. De Vasconcelos, N.D. Tran, D.P. Minh, A. Nzihou, P. Sharrock, *Compos. Interface* 22 (7) (2015) 673–687.
- [75] S.T. Oyama, X. Zhang, J. Lu, Y. Gu, T. Fujitani, *J. Catal.* 257 (2008) 1–4.
- [76] D. Chen, K.O. Christensen, E. Ochoa-Fernandez, Z.X. Yu, B. Totdal, N. Latorre, A. Monzon, A. Holmen, *J. Catal.* 229 (2005) 82–96.
- [77] J. Blanchard, A.J. Nsungui, N. Abatzoglou, F. Gitzhofer, *Can. J. Chem. Eng.* 85 (2007) 889–899.
- [78] J.J. Guo, H. Lou, H. Zhao, D.F. Chai, X.M. Zheng, *Appl. Catal. A: Gen.* 273 (2004) 75–82.
- [79] T. Hayakawa, S. Suzuki, J. Nakamura, T. Uchijima, S. Hamakawa, K. Suzuki, T. Shishido, K. Takehira, *Appl. Catal. A: Gen.* 183 (1999) 273–285.
- [80] D. Baudouin, U. Rodemerck, F. Krumeich, A. de Mallmann, K.C. Szeto, H. Ménard, L. Veyre, J.P. Candy, P.B. Webb, C. Thieuleux, C. Copéret, *J. Catal.* 297 (2013) 27–34.
- [81] K.O. Christensen, D. Chen, R. Lødeng, A. Holmen, *Appl. Catal. A: Gen.* 314 (2006) 9–22.
- [82] L. Xu, H. Song, L. Chou, *ACS Catal.* 2 (2012) 1331–1342.
- [83] K. Tomishige, Y. Chen, K. Fujimoto, *J. Catal.* 181 (1999) 91–103.
- [84] J. Wei, E. Iglesia, *J. Catal.* 224 (2004) 370–383.
- [85] J.F. Muñera, S. Irusta, L.M. Cornaglia, E.A. Lombardo, D.V. Cesar, M. Schmal, *J. Catal.* 245 (2007) 25–34.
- [86] D. Pakhare, V. Schwartz, V. Abdelsayed, D. Haynes, D. Shekhawat, J. Poston, J. Spivey, *J. Catal.* 316 (2014) 78–92.
- [87] A.M. O'Connor, Y. Schuurman, J.R.H. Ross, C. Mirodatos, *Catal. Today* 115 (2006) 191–198.
- [88] J.F. Muñera, L.M. Cornaglia, D.V. Cesar, M. Schmal, E.A. Lombardo, *Ind. Eng. Chem. Res.* 46 (2007) 7543–7549.
- [89] G.S. Gallego, C. Batiot-Dupeyrat, J. Barrault, F. Mondragoín, *Ind. Eng. Chem. Res.* 47 (2008) 9272–9278.
- [90] X.E. Verykios, *Int. J. Hydrogen Energy* 28 (2003) 1045–1063.
- [91] C. Carrara, J. Muñera, E.A. Lombardo, L.M. Cornaglia, *Top. Catal.* 51 (2008) 98–106.
- [92] S. Das, S. Thakur, A. Bag, M.S. Gupta, P. Mondal, A. Bordoloi, *J. Catal.* 330 (2015) 46–60.